CO4-1   Study of Intense Terahertz Light Source Based on Superimposing Coherent Diffraction Radiation

N. Sei and T. Takahashi[1]

Research Institute of Instrumentation Frontier, National Institute of Advanced Industrial Science and Technology
[1]Research Reactor Institute, Kyoto University

INTRODUCTION: Terahertz (THz) wave applications have developed dramatically by compact THz-wave sources based on a femtosecond laser. However, it is still difficult to identify the intermolecular vibrational modes with existing THz-wave sources, so that a THz-wave source based on an electron accelerator, which can generate an intense THz wave, has been studied flourishingly. We have planned to develop an intense THz-wave source based on a superimposing coherent diffraction radiation (CDR), which could generate a tunable-wavelength and monochromatic THz wave.

EXPERIMENTS: When a relativistic electron beam passes through a circular aperture of a metric screen, diffraction radiation (DR) is generated from the edge of the metric screen [1]. In case the wavelength of DR is longer than a bunch length of the electron beam, the DR emitted from each electron in the bunch interferes, and then intensity of the whole DR emitted from the bunch increases remarkably. Such an intense DR is called CDR. Because an electron beam is not lost by generating CDR, multiple diffraction elements can be inserted into an orbit of the electron beam to obtain intense CDR. If the multiple diffraction elements are arranged periodically, CDR emitted from each diffraction element is superimposing and the intensity of CDR emitted from the whole elements is much higher at a wavelength corresponding to the period of the elements. This is superimposing CDR that we propose.

We have conducted demonstration experiments of the superimposing CDR with an L-band electron linear accelerator at the Kyoto University Research Reactor Institute [2]. The electron-beam energy was 32 MeV and the electron charge was 0.7 nC per micropulse. The diffraction element made of brass had an aperture with a diameter of 30 mm and a depth of 0.1 mm. It also had four holes to mount itself on four poles of a diffraction element holder. A period of the diffraction elements could be adjusted by changing the widths of washers which were mounted on the poles, as shown in figure 1. When the period was 3 mm, the holder could attach the diffraction elements of 20 or less sheets. The holder was located 0.5 m upper stream from an aluminum foil. To avoid the electron beam colliding with the diffraction elements, an iron aperture which has a hole of 30 mm diameter and a width of 40 mm, was installed behind a titanium window. A permanent bending magnet was also installed at 0.2 m downstream from the holder, and it deflected the electron beam by 7.5 degrees. The CDR beam generated by the
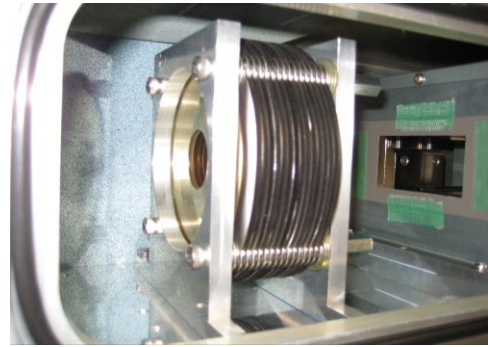

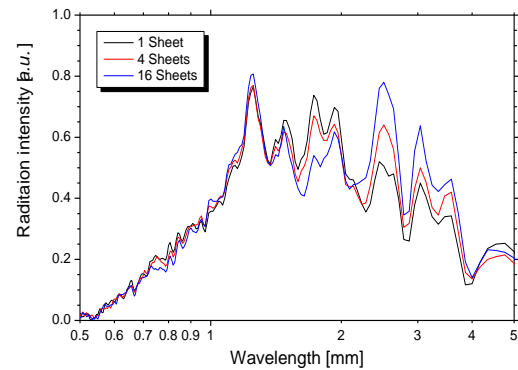Fig. 1   Photograph of the diffraction element holder.

Fig. 2   Spectra of the radiation from the diffraction elements.

diffraction elements was transported by mirrors to the experimental room, and a spectrum of the CDR beam was measured by a Martin-Puplett-type interferometer. Figure 2 shows the observed spectra when the number of the diffraction elements was 1, 4, and 16. The interval of the diffraction elements was 2.9 mm. Radiation power around a wavelength of the interval became larger as the number of the diffraction elements increased. This experimental result suggests that the CDR emitted from each diffraction element was superimposed. However, total radiation power hardly depended on the number of the diffraction elements. It is noted that the CDR power was much smaller than coherent transition radiation power emitted from the titanium window.

CONCLUSIONS: The superimposing CDR has been observed by multiple diffraction elements. We will examine an optical pass which will extract only the CDR beam efficiently, and demonstrate wavelength tunability of the CDR.

REFERENCES:
[1] Y. Shibata *et al.*, Phys. Rev. E., **52** (1995) 6787.
[2] T. Takahashi and K. Takami, Infrared Phys. Technol., **51** (2008) 363-366.

CO4-2   Metal Ion Adsorption by Acrylic Acid Grafted PET Films Prepared by γ Irradiation

N. Rahman, N. Sato[1], Y. Oba[1], M. Sugiyama[1],
T. Miyazaki, Y. Hidaka, H. Okabe and K. Hara

Department of Applied Quantum Physics and Nuclear Engineering, Kyushu University
[1]*Research Reactor Institute, Kyoto University*

INTRODUCTION: In recent years discharge of hazardous heavy metals in industrial effluents and their removal have received much public attention [1]. But the conventional methods used for heavy metal waste water treatment such as precipitation, ion exchange, activated carbon adsorption, electrolytic method etc. have limitations like high cost, low removal rate or difficulty for regeneration and reuse. Therefore many researches focused on the study of alternative low cost effective adsorbents. In the present work AAc grafted PET films were prepared by γ irradiation and after hydrolysis through KOH treatment the grafted films were used to study the adsorption of Cu(II), Co(II) and Ni(II).

EXPERIMENTS: The dry PET films weighing $W_{pristine}$ were taken into glass bottles containing different concentration (20- 40 wt %) of AAc aqueous solutions. $FeCl_3$ at a constant concentration (1 wt %) was added to the AAc solutions to minimize homopolymer formation. The contents of the glass bottles were then irradiated with different doses (20-100 kGy) of γ rays with a dose rate of 1.0 kGy/h in air (γ-ray irradiation of the PET films was carried out at the ^{60}Co γ-ray irradiation facility of Research Reactor Institute, Kyoto University). The obtained grafted films were washed in distilled water at 60°C for 24 h to remove the homopolymers. Then the films were dried in a vacuum oven at 60°C for 24 h and were weighed ($W_{AAc\ grafted}$). The graft yield was determined by the percent increase in the weight as follows:
Graft yield:
$\delta W_{AAc\ grafted} (\%) = (W_{AAc\ grafted} - W_{pristine}) / W_{pristine} \times 100$.

The AAc grafted films with 40 % graft yield (obtained at 40 % AAc concentration and 100 kGy dose) were modified by treatment with 2.5 % KOH for 2 min at 25 °C. The modified AAc grafted films of 60 mg were soaked into the 10 ml aqueous solutions including of Cu(II), Ni(II) and Co(II) at a definite metal ion concentration and pH for 60 min at room temperature (25 °C). pH of the solutions were adjusted using HCl and NaOH solution. Metal loaded films were washed and dried. The metal-ion concentrations of the solutions were analyzed by ICP-MS.

The metal ion uptake capacity of the film was calculated as follows:
$$Q = V(C_1\text{-}C_2)/W ,$$
where Q is the adsorption amount (mg/g), W the weight of the film (g), V the volume of solution (L), and C_1 and C_2 are the concentrations (mg/L) of metal ion before and after adsorption respectively.

RESULTS: The prepared AAc grafted films (G- 40 %) were modified by treatment with KOH which increased the metal ion adsorption capacity of the films largely, almost 10 times than the AAc grafted films. The adsorption capacity of Cu(II), Co(II) and Ni(II) ions obtained in the present study are presented in Table 1. The modified AAc grafted PET films after adsorption of Cu(II), Co(II) and Ni(II) ions are shown in Figure 1.

Table 1. Cu(II), Co(II) and Ni(II) adsorption capacity of AAc grafted and hydrolyzed AAc grafted PET film (From single metal solutions)

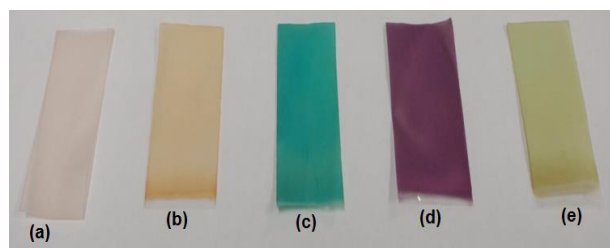| Adsorbent film	Cu(II) adsorption capacity (mg/g)	Co(II) adsorption capacity (mg/g)	Ni(II) adsorption capacity (mg/g)
AAc graft PET	10.0	7.0	8.0
Hydrolyzed AAc graft PET	100.0	67.0	85.0

Fig. 1: (a) AAc grafted PET (b) AAc grafted PET after modification by KOH treatment (c) Modified AAc grafted PET film after Cu(II) loading (d) Modified AAc grafted PET film after Co(II) loading (e) Modified AAc grafted PET film after Ni(II) loading.

REFERENCES:
[1] J. Ui (Ed.), Industrial Pollution in Japan (The Japanese Experience Series), United Nations University Press, Tokyo, 1992
(Full text is also available at
http://www.unu.edu/unupress/unupbooks/uu35ie/ uu35ie00.htm.).

CO4-3 Structural Determination by Ultra Small Angle Light Scattering of Self-Assembled Complexes to Perform Small Angle Neutron Scattering Experiments

S. Sato, N. Sato[1] and M. Sugiyama[1]

WPI-AIMR, Graduate School of Science, and ERATO (JST) at Tohoku University
Research Reactor Institute, Kyoto University

INTRODUCTION: Self-assembled metal-organic complexes have advantages that huge, well-defined structures can be synthesized in simple synthetic methods with designable substituents introduced by precise organic syntheses. Our group has focused on the construction of new molecular frameworks of metal-organic complexes and reported the first stellated polyhedral structures [1], sphere-in-sphere structures [2], extended spherical structures [3], and so on. In the course of one-step syntheses of self-assembled complexes, we noticed that step-wise assembly can be also designed through the peripheral functional groups on complexes.

Self-assembled complexes with π-stacked motifs [4] are interesting targets not only from the viewpoints of their unique structures but also from those of NMR applications based on their magnetic behaviors. We found that the complexes show magnetic aligning dynamics due to the parallel accumulation of large π-moieties in a molecule [5]. Here, we envisioned that the introduction of hydrophilic substituents on the complexes would improve the solubility of the complexes in water and accellerate the further intermolecular π-stacking in solution. The assembled structures could be analyzed by small angle neutron scattering (SANS) and the preliminary structural information could be derived from ultra small angle light scattering measurements on lab equipments.

RESULTS: A series of π-stacked complexes with variety of hydrophilic substituents were synthesized as showin in Fig. 1. The structures were detemined by NMR and the framework with stacked π-moieties was unambiguously determined by single crystal X-ray diffraction studies. When we compared the solubility of the newly synthesized complexes with that of previously reported structure with less hydrophilic substitutents, significant improvement of the solubiity was confirmed, proving that the molecular design was successful. We found that the complexes show larger assembled structures in more concentrated solution presumably due to intermolecular π-stacking. The more assembled structures showed smaller diffusion coefficients estimated by 2D NMR measurements. Rough size was estimated by ultra small angle light scattering, showing consistent structures with NMR analyses. The detailed assembled structures would be determined by precise SNAS methods, which will also give the conformational information of the attached substituents.
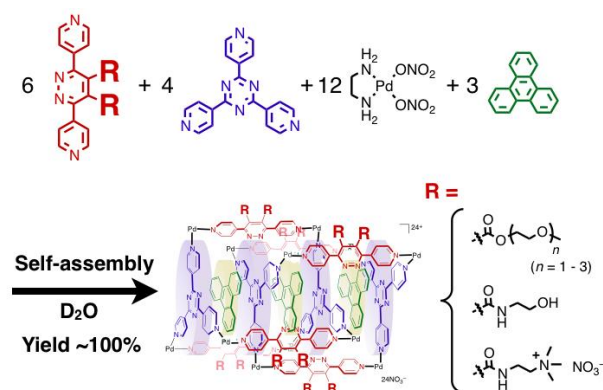

Fig. 1. Representative scheme for the self-assembly of π-stacked complexes from six bidentate ligands (red), four tridentate ligand (purple), twelve palladium (II) ions with 90°–corner cap, and three guest organic molecules. The twenty five components disolved in water assemble into a metal-organic complex with a single structure in 100% yield. A variety of substituent groups, R, was introduced by the organic functionalization on the bidentated ligand, affording the correspoinding functionalized metal-organic complexes, where the position and number of the funcioal groups are clearly defined by the mother framework of the assembled complexes.

EXPERIMENTS: The building blocks of the self-assembled products were purchased from chemical company or synthesized according to basic organic synthtic procedures which will be reported elsewhere. The building blocks were mixed in a stoichiometric molar ratio and dissolved in D₂O. The structures of the products were determined mainly by NMR and by other analytical methods. The diluted samples were prepared with water, and the solution was checked by NMR to confirm the maintenance of the frameworks.

REFERENCES:
[1] Q.-F. Sun *et al.*, Nature Chem., **4** (2012) 330-333.
[2] Q.-F. Sun *et al.*, Angew. Chem. Int. Ed., **50** (2011) 10318-10321.
[3] Q.-F. Sun *et al.*, Science, **328** (2010) 1144-1147.
[4] Y. Yamauchi *et al.*, J. Am. Chem. Soc., **132** (2010) 9555–9557.
[5] S. Sato *et al.*, J. Am. Chem. Soc., **132** (2010) 3670–3671.

Current Status of B–3 Beam Port of KUR

K. Mori, H. Yoshino, T. Fukunaga, Y. Kawabata, S. Sato[1], H. Hiraka[1], Y. Yamaguchi[2] and K. Iwase[3]

Research Reactor Institute, Kyoto University (KURRI)
[1]High Energy Accelerator Research Organization (KEK)
[2]Institute for Materials Research, Tohoku University
[3]Department of Materials and Engineering, Ibaraki University

INTRODUCTION: The B–3 beam port of Kyoto University Research Reactor (KUR) had long been used as a four-circle single-crystal neutron diffractometer (4CND). For the last decade, however, the 4CND was so old that its research activity on neutron science was quite low. Therefore, the 4CND needed to be replaced and the increasing demand for a new neutron diffractometer (Compact multipurpose neutron diffractometer) calls for the structural investigations using neutron diffraction. Here, we report the current status of the B-3 beam port of KUR.

NEUTRON DIFFRACTION: The compact multipurpose neutron diffractometer is now being installed on the B–3 beam port. The neutron wavelength (λ), which is monochromatized by the (220) plane of a Cu single crystal, is 1 Å. To cover the detector area (6 º $\leq 2\theta \leq$ 150 º), 24 ^{3}He tube detectors (1/2 inch in diameter) have been prepared. The distances from the monochromator to the sample and from the sample to the detector will be 1.9 m and 1.2 m, respectively. To assess the neutron beam properties of the B-3 beam port, the preliminary neutron diffraction experiments using Ni powder were performed. As shown in Fig. 1, we observed their several Bragg reflections, which could be indexed on the basis of λ = 1 Å.
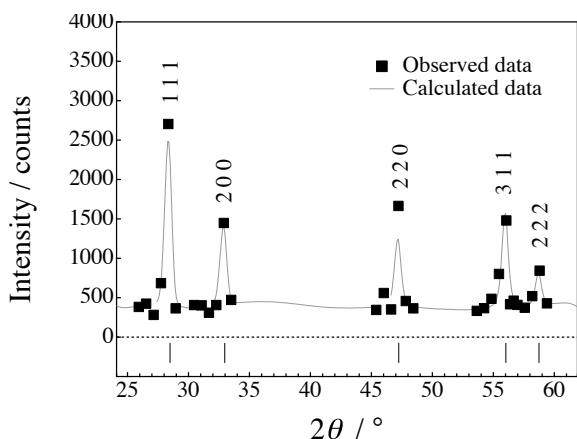

Fig. 1. Neutron diffraction data of Ni powder collected at the B-3 beam port of KUR.

NEUTRON DETECTOR SYSTEM: The data acquisition group of the neutron science division of KEK (KEK–KENS DAQ group) has used the B–3 beam port to assess their new ^{6}Li-glass neutron detector system, LiTA12. The LiTA12 system consists of a ^{6}Li-glass neutron detector with a multianode photo multiplier tube (MA–PMT), an amplifier, and an analog-to-digital converter (ADC) board. The B–3 beam port has a wide space around the sample position; therefore we can easily install any other system like the LiTA12 system (see Fig. 2).
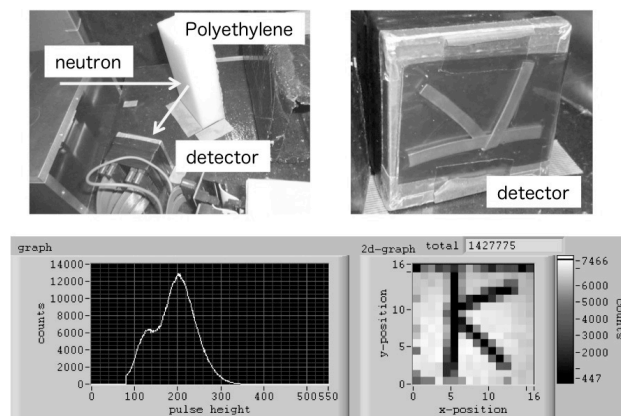

Fig. 2. New ^{6}Li-glass neutron detector system, LiTA12, developed by the KEK–KENS DAQ group. The "K" was made of cadmium plates.

NEUTRON MONOCHROMATOR: The development of large crystal monochromators for a polarized neutron beam has been conducted by the KEK–Tohoku University group. To assess their crystal monochromators, they have used the B–3 beam port. Figure 3 shows the neutron rocking curve of the cold-pressed Cu single crystal ((200) plane). The further investigations are now in progress.
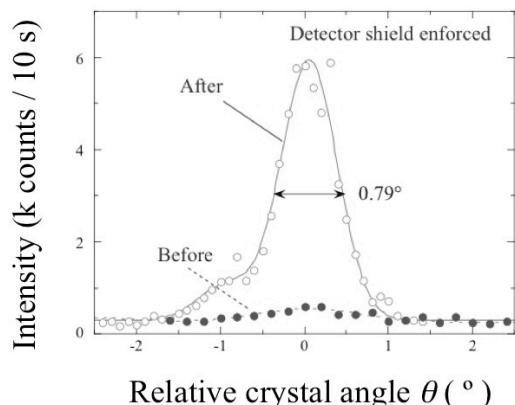

Fig. 3. Neutron rocking curve of the cold-pressed Cu single crystal – (200) plane.

Sub-Terahertz Absorption of Ionic Liquid

T. Awano and T. Takahashi[1]

Faculty of Engineering, Tohoku Gakuin University
[1]Research Reactor Institute, Kyoto University

INTRODUCTION:
We have observed millimeter wave absorption bands around 6 and 8 cm^{-1} in AgI-superionic conductive glasses. These bands were also observed in CuI-superionic ones[1-3]. These bands seems to be due to collective motion of conductive ions, although how conduction ions moves in correlation is not clear.
Ionic liquid is molten salt at room temperature. It is interesting to compare ionic motion in ionic liquids with those in superionic conductor.

EXPERIMENTS:
Ionic liqids N,N-Diethyl-N-methyl-N-(2-methoxyethl) ammonium tetrafluoroborate ([DEME][BF$_4$]) and N,N-Diethyl-N-methyl-N-(2-methoxyethl)ammonium bis(trifluoromethanesulfonyl)imide ([DEME][TFSI]) (Kanto Chem. co., inc.) were spread into filter paper. Transmission spectra of single and double papers with ionic liquids were measured at room temperature and low temperatures. Absorption spectra were obtained by subtraction of them.

RESULTS: Fig. 1 shows absorption spectra of [DEME][BF$_4$]. This ionic liquid becomes solid under 282K (crystal). Fig. 2 shows absorption spectra of [DEME][TFSI]. This ionic liquid becomes solid under 182K (glass). Two absorption bands were observed around 6 and 8 cm^{-1}, which are almost coincident with those in AgI-superionic conductive glasses. These bands have almost equal peak positions and intensities in both ionic liquids. This means that these absorption bands are due to cation motion, which are common in these liquids. However, temperature dependence of these bands are different between these ionic liquids. This difference seems to be due to the difference of their phase transition temperatures and solid states.

REFERENCE:
[1] T. Awano and T. Takahashi, J. Phys. Conf. Ser., **148** (2009) 012040/1-4.
[2] T. Awano and T. Takahashi, J. Phys. Soc. Jpn. **79** Suppl. A (2010) 118-121.
[3] T. Awano and T. Takahashi, Proceedings of the 13th Asian Conference on Solid State Ionics, (2012) 569-576.
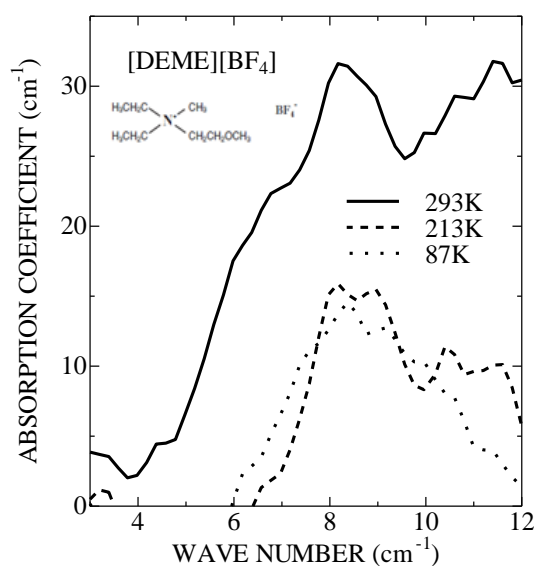

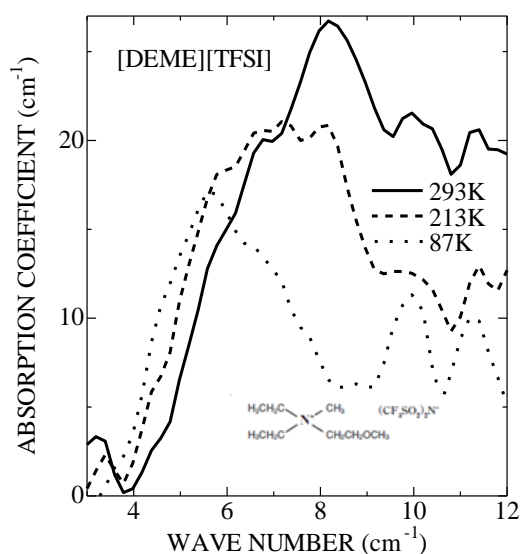Fig. 1. Absorption spectra of N,N-Diethyl-N-methyl-N-(2-methoxyethl)ammonium tetrafluoroborate.

Fig. 2. Absorption spectra of N,N-Diethyl-N-methyl-N-(2-methoxyethl)ammonium bis(trifluoromethanesulfonyl)imide.

CO4-6   Synthesis of Metal Nanoparticles under the Gamma-ray Irradiation Field

F. Hori, K. Nagata, T. Hori, N. Kobayashi, A. Iwase and M. Sakamoto[2]

Dept. of Mater. Sci., Osaka Prefecture University
[1]*Research Reactor Institute, Kyoto University*

INTRODUCTION: Metal nanoparticles have different properties from bulk ones are known. Therefore, the nanoparticles are excellent optical properties, thermal properties, and so on. In particular, the development of new functional nanoparticles with different properties depending on the purpose is expected. Au nanoparticles with rod shape have two surface plasmon resonance (SPR) absorption peaks in the visible and infrared range. Moreover, the multi component alloy nanoparticles may have different characteristic features compared to that for pure elemental nanoparticles. There are many reports for synthesis and characterization of pure Au nanorods, but it is difficult to control the size, aspect ratio and alloy mixing structure for multi-alloy nanorods. On the other hand, unique structural of nanoparticles have been synthesized in metallic ions solutions under various kinds of irradiation fields, such as ultrasonic, electron, gamma-ray and heavy ion [1]. Au nanorods have often been synthesized by the seed-mediated chemical reduction method for Au ions in their water solution. We have reported that synthesis of Au nanorods by using gamma-ray irradiation without any seed materials [2]. In this study, therefore, we tried synthesis of Au-Pd binary alloy nanorod under gamma-ray irradiation reduction field.

EXPERIMENTS: Aqueous solutions including $NaAuCl_4 \cdot 2H_2O$ (Au^{3+} ion), silver nitrate, dilute sulfuric acid, ascorbic acid and cetyl trimethyl ammonium bromide (CTAB) were argon purged and sealed into polystyrene vessel. They were irradiated by gamma-ray from ^{60}Co radioactive source with total dose of 6.0 kGy at about 298 K (the first step: (a)), followed by the adding of $PdCl_2 \cdot 2NaCl \cdot 3H_2O$ (Pd^{2+} ion) and the irradiation of the solution with total dose of 6.0 kGy again (the second step: (b)). The dose rate was fixed to 5.3 kGy/h. Generated nanoparticles were investigated by UV/vis absorption spectroscopy and transmission electron microscope (TEM). UV–vis absorption spectra were measured by using Shimadzu UV-2550 spectrophotometer in the wavelength range in 300–800 nm. Also, the structure and chemical analysis of nanoparticles were examined by conventional TEM JEOL JEM-200CX, 2000FX, and Scanning-TEM with energy dispersive X-ray analysis (EDX) apparatus.

Samples for TEM observations were made by putting a drop of colloidal solutions on a carbon film with a Mo mesh and dried them in a vacuum.

RESULTS: Figure 1 shows that rod shape of nanoparticles were fabricated by gamma-ray irradiation for the solutions containing only gold ions and for after added of palladium ions into them and irradiated continually. The Au nanorods have an average length of 14 nm and an average aspect ratio is about 3. The nanorods after Pd ion reduction have an average length of 13 nm and an average aspect ratio is about 3. No growth of nanorods can be observed between (a) and (b). On the other hand, optical feature of these nanorods, which is characterized by a SPR peak at 740 nm in absorption spectra for Au nanorods, move to 700 nm. As shown in Fig. 2, the result of EDX analysis clearly shows that nanorod is constructed by Au nanorod surrounded by thin Pd surface layers, even though the size and aspect ratio does not change. Taking into account for these results, SPR band of nanorods changes only by coverd by 0.7 nm Pd layrs.
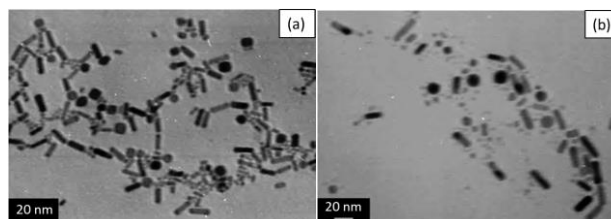

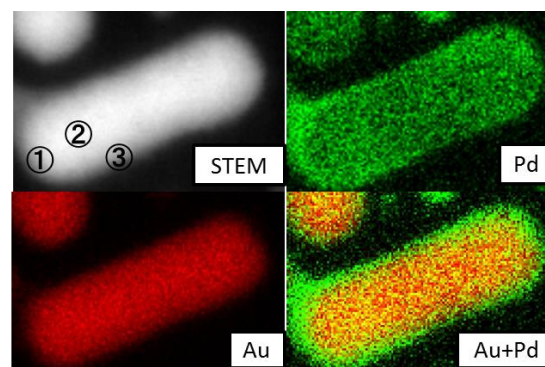Fig. 1 TEM images of (a) Au nanorods and (b) Au-Pd nanorods.

Fig. 2 EDX mapping for Au-Pd nanorods synthesized by two step γ-ray irradiation reduction.

REFERENCES:
[1] N. Taguchi *et al.,* Appl. Surf. Sci. vol.**255** (2008) 164−166.
[2] A. Okamoto *et al.,* Jap. J. Appl. Phys. **51** (2012) 1049−1053.

CO4-7 Radiation-Induced Luminescence for Applying to Retrospective Dosimetry

H. Fujita, M. Sakamoto[1] and T. Saito[1]

Nuclear Fuel Cycle Engineering Laboratories, JAEA
[1]Research Reactor Institute, Kyoto University

INTRODUCTION: An irradiated quartz emits radiation induced luminescence such as thermoluminescence (TL) and optically stimulated luminescence (OSL). The luminescence phenomena have been used for retrospective dosimetry [1, 2] and dating of sediments, etc. However, the luminescence emission mechanism from Japanese natural quartz has not yet been well explained. In this study, the emission mechanisms of TL and OSL were investigated in conjunction with various radiation-induced phenomena after annealing treatments of quartz samples, involving TL, OSL and electron spin resonance (ESR) measurements.

EXPERIMENTS: Natural quartz grains (150~250 μm) were extracted from surface soils by a general treatment of 6M hydrochloric acid (HCl), 6M sodium hydroxide (NaOH) and concentrated hydrofluoric acid (HF) with hand selection for the sake of elimination of feldspar grains as low as possible under a microscope. The quartz samples were annealed at 800ºC for 24 hours in an electric furnace. The annealed quartz samples were irradiated a dose of 1 kGy with ^{60}Co source at room temperature at Kyoto University Research Reactor Institute (KURRI). The irradiated sample was stored at room temperature for one day to eliminate afterglow emission in dark room. The ESR measurement was carried out using an ESR spectrometer (Jeol Ltd., JES-TE 200) at room temperature and −196ºC, respectively. Prior to the ESR measurements, the quartz samples were annealed for 1 min at 50ºC intervals ranging from 150 to 300ºC as preheat treatment. After the ESR measurements, all luminescence measurements were performed using a JREC automated TL/OSL-reader system installed with a small X-ray irradiator (Varian, VF-50J tube). All preparations were carried out under dim red light.

RESULTS: In this research, the ESR signals of Ti-centers ($[TiO_4/H^+]^0$, $[TiO_4/Li^+]^0$ and $[TiO_4/Na^+]^0$), Al-centers and RT-centers were detected in the annealed quartz samples. Both ESR signal intensities of Ti-centers

and Al-centers were decreased with the preheating temperatures depended on their centers as shown in Fig.1. On the other hand, intensities of RT-centers were disappeared with the preheat treatment. Their results agreed to our previous results.
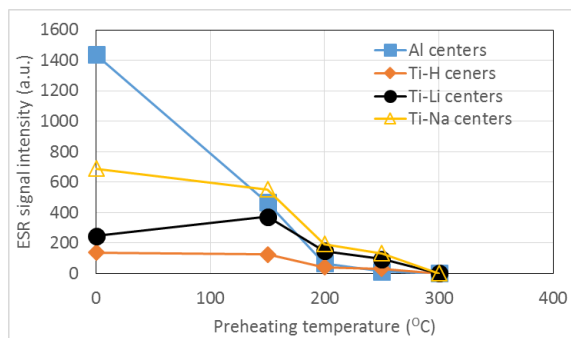

Fig.1.
Tendency of ESR signal intensity with preheating temperature.

It is suggested that Al-center and RT-center are hole-trapped centers and Ti-centers are electron-trapped centers. In TL glowcurve, some electron-trapped centers should control peak position and some hole-trapped center should control emission wavelength. In TL measurement results, ultra-violet TL (UVTL) and red TL (RTL) intensities integrated in all glowcurve area decreased with preheating temperature. Finally, their TL emissions were disappeared at 300ºC. The results agreed to tendency of the Ti-center and Al-center intensities. On the other hand, OSL intensity was not related to the tendency of the ESR centers at all. The reason why the tendency of OSL intensity showed different from the tendency of TL intensity would be the re-trapping effect influenced by the preheat treatment.

In this research, the luminescence emission mechanism could not be identified. Therefore, further work is necessary to identify luminescence mechanism using ESR measurement and annealing experiment.

REFERENCES:
[1] H. Fujita *et al.*, Radiation Measurements, **46** (2011) 565–572.
[2] Hiroki Fujita, Radiation Physics and Chemistry, DOI: http://dx.doi.org/10.1016/j.radphyschem.2014.01.001.

CO4-8

Absorption Spectroscopy with the Coherent THz Radiation from Linac Electron Beams

S. Okuda, H. Saito and T. Takahashi[1]

Radiation Research Center, Osaka Prefecture University
[1]Research Reactor Institute, Kyoto University

INTRODUCTION: The coherent transition radiation (CTR) from electron bunches of a linear accelerator (linac) have continuous spectra in a submillimeter to millimeter wavelength range and extremely high peak-intensities. The light sources using the CTR have been applied to absorption spectroscopy [1-4]. However, the number of such light sources is very limited. The light source system using the CTR from the electron beams of the 45 MeV L-band electron linac has been established at KURRI [5]. The CTR light sources developed have been applied to absorption spectroscopy especially for matters with relatively strong light absorbance such as water.

In the present work the light path of the CTR light source has been modified and absorption spectroscopy has been carried out for water and aqueous solutions.

CHARACTERISTICS OF THE CTR: The CR is emitted as a pulsed and polarized light. The pulse structure of the CR corresponds to that of the electron beam from the linac. The light can produce the intense pulsed electric field and would cause the excitation in a matter. The spectrum of the CTR is determined by the micro-pulse shape of the electron bunch.

EXPERIMENTAL METHOD: The experimental configurations for the absorption spectroscopy are schematically shown in Fig. 1. The output CTR light from a
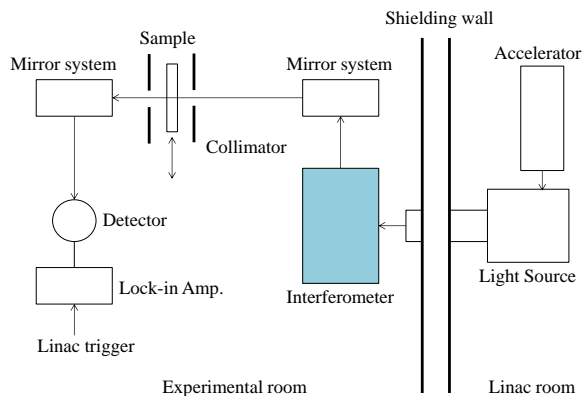

Fig. 1. Schematic diagram showing the configurations for absorption spectroscopy using the CTR.

light source chamber was transported out from the accelerator room. The spectrum of the light after passing through the sample was measured with a Martin-Puplett type interferometer and a liquid-He-cooled silicon bolometer. The sample was located on the light path between the interferometer and the detector [5]. The light was focused at a light collimator 8 mmϕ in diameter located before the sample. In this experiment the diameter

of the light after the sample was measured and the sample holder was modified not to interrupt the transmission of light through the holder.

The spectrum was sufficiently stable during the measurements within ±1-1.5% in a wavenumber range of 3-13 cm^{-1}. The wavenumber resolution was 0.2 cm^{-1}. The details of the measurements are described in ref. 5.

The samples were water and aqueous solutions of NaCl and glucose.

RESULTS AND DISCUSSION: The wavenumber dependence of the transmittance of light measured for water obtained by averaging over four measurements is shown in Fig. 2 along with the schematical configurations around the sample. The thickness of the water sample was about 120 μm, which was sandwiched with two anhydrous quartz plates 3 mm thick.
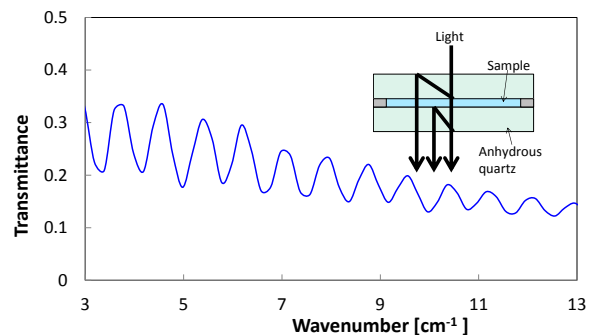

Fig. 2. Wavenumber dependence of the transmittance of the CTR light for water and the schematic configurations around the sample.

The periodical oscillation on the curve can be attributed to the interference between the incident and reflected lights as shown in this figure. The refractive index and the absorbance of water can be obtained by analyzing the results.

The new system for the pump-probe experiments by using the 16 MeV S-band linac in Osaka Prefecture Uiversity has been developed [6]. This will be applied to investigating the transient phenomena induced by the pulsed CTR or electron beams using the CTR as probe.

REFERENCES:
[1] T. Takahashi *et al.*, Rev. Sci. Instrum. **69** (1998) 3770.
[2] K. Yokoyama, Y. Miyauchi, S. Okuda, R. Kato and T. Takahashi, Proc. 20th Int. Free-Electron Laser Conf. (1998, Williamsburg, USA) II 17-18.
[3] S. Okuda, M. Nakamura, K. Yokoyama, R. Kato and T. Takahashi, Nucl. Instrum. Meth. **A445** (2000) 267.
[4] S. Okuda *et al.,* Radiat. Phys. Chem. **75** (2006) 903.
[5] S. Okuda and T. Takahashi, Infrared Phys. Technol. **51** (2008) 410.
[6] S. Okuda, T. Kojima, R. Taniguchi, Proc. XXV Linear Accelerator Conf. (2010, Tsukuba, Japan) 79-81.

^{57}Fe Mössbauer Studies of Superconducting $Sr_2VFeAsO_{3-d}$ and Heavy Fermion $CeRu_{1-x}Fe_xPO$

Y. Tojo, T. Nakamura, M. Matoba, S. Kitao[1], M. Seto[1] and Y. Kamihara

Department of Applied Physics and Physico-Informatics, Keio University
[1]Research Reactor Institute, Kyoto University

INTRODUCTION: A hyperfine fields B_{hf} experienced by nuclei of atoms at crystallographic sites in magnetic and/or antiferromagnetic metals are of interest in view point of hyperfine interactions and important for their use in the determinations of nuclear magnetic dipole moments by a variety of methods including those based on low-temperature nuclear orientation. Guang-Han Cao et al reported that $Sr_2VFeAsO_{3-d}$ is an FeAs-based superconductor, which reveals antiferromagnetic under 150 K originating in local d-electron moments of vanadium, and the superconducting transition temperature T_c is 24 K.[1] In $Sr_2VFeAsO_3$-phase, surplus electrons that come from oxygen defects in block layers become conduction electrons in FeAs layers, which turn into cooper pairs in superconducting phase. In the meantime, C. Krellner et al reported that CeRuPO is a heavy fermion, which reveals ferromagnetism under 15 K.[2] Our group reported that CeFePO is a paramagnetic heavy fermion, which has no magnetic transition down to 2 K.[3]

In this report, element-specific magnetism and electronic phase of Fe sublattice in $Sr_2VFeAsO_{3-d}$ are elucidated using ^{57}Fe Mössbauer spectroscopy.[4] We also demonstrate the several physical properties near ferromagnetic quantum critical point applying ^{57}Fe Mössbauer spectroscopy to the samples of x=0.25, 0.50, 0.80, 0.85, 0.87, 0.95 of $CeRu_{1-x}Fe_xPO$.[5]

EXPERIMENTS: Polycrystalline samples of $Sr_2VFeAsO_{3-d}$ were prepared by the solid-state reactions in a sealed silica tube using dehydrated SrO, FeAs, V_2O_5, V as starting materials, reported previously.[6] Polycrystalline sample of $CeFe_{1-x}Ru_xPO$ (x = 0.00, 0.05, 0.10, 0.20, 0.25, 0.50, 0.75) was prepared by a two-step solid-state reaction, similar to LnFePO (Ln = La, Ce)[7,8] using dehydrated CeO_2 and two mixtures of compounds, Ce-2Fe-2P and Ce-2Ru-2P powders as starting materials. The dehydrated CeO_2 was prepared by heating commercial CeO_2 powder (Nippon Yttrium; 99.9 wt.%) at 800 °C for 5 h in air. To obtain Ce-2Fe[Ru]-2P powder, Ce (Nippon Yttrium; 99.9 wt.%), Fe (Kojundo Chemical Laboratory; 99.99 wt.%) [Ru (Nilaco; 99.9+ wt.%)], and P (Kojundo Chemical Laboratory; 99.999 wt.%) were mixed in a stoichiometric ratio of 1:2:2 and heated at 400 °C for 40 h and 800 °C for 10 h in an evacuated silica tube. Then, a mixture of the three powders (dehydrated CeO_2, Ce-2Fe-2P, and Ce-2Ru-2P powders) was pressed into pellet and heated in doubly sealed silica tubes at ~1300 °C for 40 h. All procedures were carried out in an Ar-filled glove box (MIWA Mfg; O_2, H_2O < 1 ppm). The first process was effective in preventing the selective oxidation of the Ce metal. The silica tube in the second heat treatment was filled with 0.16-0.2 atm pressure of high-purity Ar gas at room temperature to prevent an implosion of the silica tube. Ru content x is determined by nominal value. The crystal phase of the obtained product was examined by powder X-ray diffraction (XRD;RigakuRINT-2500) using CuKα radiation. Almost all the diffraction peaks are assigned to the $CeFe_{1-x}Ru_xPO$ phase. Electrical resistivity measurements were performed at 2–300 K by a dc four-probe technique using silver paste as electrodes. Magnetization measurements were performed for polycrystalline samples using a Quantum Design magnetic properties measurement system (MPMS). The ^{57}Fe Mössbauer (MS) experiment on the two series of compounds, $Sr_2VFeAsO_{3-d}$ and $CeRu_{1-x}FexPO$, was performed with conventional ^{57}Fe MS equipment using 14.4 keV γ-rays from a ^{57}Co source in an Rh matrix.

RESULTS: ^{57}Fe MS to the samples of d=0.20, 0.50, 0.70 of $Sr_2VFeAsO_{3-d}$ were measured and analyzed for obtaining quantitative value of B_{hf}. As a result, the existence of spin density wave phase near superconducting phase was clarified and elucidated. The result indicates that spin fluctuations developed at the boundary of the spin density wave may be driving force behind superconductivity in $Sr_2VFeAsO_{3-d}$.

^{7}Fe MS of the samples of $CeRu_{1-x}Fe_xPO$ were measured and analyzed for obtaining both of isomer shift (IS) and Debye temperature (θ_D). Both of IS-x and θ_D-x curves show an anomaly at quantum critical points x~0.13. These results indicate that the dimensionality of the system is tuned from 3 to 2 by Fe-doping driving to paramagnetic phase, and that Kondo breakdown occurs at the quantum critical point reconstructing Fermi surface. [9] Though there are reports that demonstrate anomaly of physical properties at antiferromagnetic quantum critical point, this is the first report that demonstrates anomaly of (IS & θ_D) at ferromagnetic quantum critical point using ^{57}Fe MS.

REFERENCES:
[1] G. H. Cao *et al.*, Phys. Rev. B **82**, 104518 (2010).
[2] C. Krellner *et al.*, Phys. Rev. B **76**, 104418 (2007).
[3] T. Nakamura *et al.*, J. Phys. Soc. Jpn. **81**, 064714 (2012).
[4] Y. Tojo, Y. Kamihara *et al.*, unpublished.
[5] T. Okano, T. Nakamura, Y. Kamihara, M. Matoba *et al.*, unpublished.
[6] Y. Tojo *et al.*, J. Appl. Phys. **113**, 17E157 (2013).
[7] Y. Kamihara *et al.*, J. Am. Chem. Soc. **128**, 10012 (2008).
[8] Y. Kamihara *et al.*, J. Phys. Chem. Solid **69**, 2916 (2008).
[9] S. Kitagawa *et al.*, J. Phys. Soc. Jpn. **82**, 033704 (2013).

Characterizations of Dynamic Behavior for Organic Solar Cells under High-Energy Photons and Secondary Electrons by ^{60}Co Beams

M. Oita, K. Nakata[1] and K. Sakurai[2]

Graduate School of Health Sciences, Okayama University
[1]*Department of Applied Biological Science, Faculty of Science and Technology, Tokyo University of Science*
[2]*Research Reactor Institute, Kyoto University*

INTRODUCTION: The development of solar cells has been expected to make important contributions of the solution of the energy problem. Photovoltaics has been dominated by solid-state junction devices, usually made from crystalline or amorphous silicon. In recent years, the possible advantages of organic semiconductors are remarked as low cost fabrication and roll-to-roll manufacturing on flexible substrat [1-4]. Many applications of these devices are expected to use for not only energy solutions but for radiation dosimetry. Si-based semiconductor detectors are often used for medical applications of radiation dosimetry [5,6]. Therefore, organic solar cells (OSC) would be possible for the evaluation of radiation dose such as radiation examinations and radiotherapy. In this work, the authors investigated the degradations and tolerance of two types of OSCs compared to single-crystal Si-based solar cells (Si-SCs) under high-energy secondary electrons by ^{60}Co beams.

EXPERIMENTS: The samples used in this work are Si-SCs (#0906005B, Mimatsu Audio Corp, Japan) and OSCs. The surfaces of Si-SCs are coated with epoxy resin. OSCs fabricated by TiO_2 photoelectrodes which were prepared by screen-printing TiO_2 paste (Ti-Nanoxide T/SP, Solaronix SA) on fluorine-doped indium tin oxide/glass (FTO) substrates (Solaronix SA). The TiO_2 photoelectrodes were annealed at 200 °C for 10 min, and then at 500 °C for 30 min, resulting in anatase films. Multiple heating steps were performed to avoid cracking of the TiO_2 layer. The above TiO_2 photoelectrode was soaked in a solution of dyes, which were derivatized with ruthenium (N719) [7] or metal-free indoline (D149) [8] and then dried under an air flow. A 50-µm-thick Himilan (R) film was used to assemble the TiO_2 electrode with a Pt-sputtered FTO electrode (the thickness of the Pt layer was 100 nm). The space between the electrodes was filled with a mixed electrolyte in acetonitrile. All of the samples were irradiated by ^{60}Co beams ranged from 50 Gy to 150 kGy at KUR ^{60}Co Gamma-ray Irradiation facility. To evaluate the degradation of the samples, the conversion efficiencies and other electrical characteristics were measured by a solar simulator (YSS-T150A, YAMASHITA DENSO Corp.).

RESULTS: Figure1 shows the degradation of conversion efficiencies for OSCs as compared to Si-SCs by radiation. There were no significant changes between OSCs and Si-SCs less than 5 kGy. Fig.2 shows the degradations of conversion efficiencies for two types of OSCs by radiation. The degradations of the efficiencies for both OSCs were observed about less than 1%/kGy. However, significant difference between dyes of N719 and D149. In summary, the radiation tolerance of OSCs by high-energy photons and electrons by ^{60}Co beams were investigated. The results showed that the dosimetry devices using OSCs would be feasible for medical application.
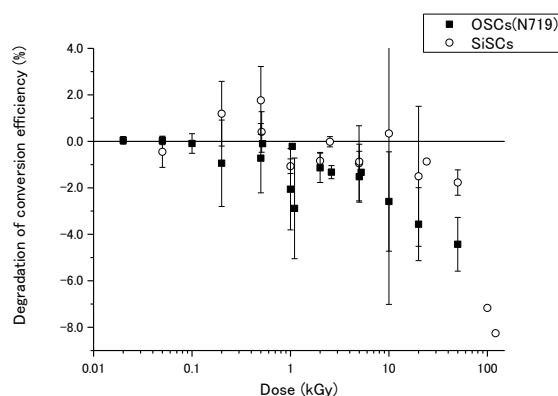

Fig. 1. The degradation of conversion efficiency for OSCs (N719) and Si-SCs under secondary electrons by ^{60}Co beams.
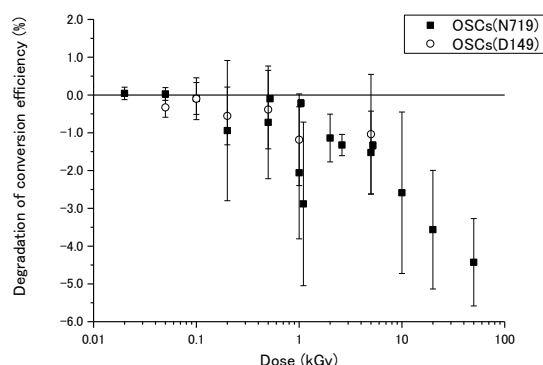

Fig. 2. The degradation of conversion efficiency for two types of OSCs under secondary electrons by ^{60}Co beams.

REFERENCES:
[1] Grätzel, M., Nature, **414** (2001) 338-344.
[2] Hagfeldt, A. *et al.*, Acc. Chem. Res., **33** (2000) 269-277.
[3] M. Manceau *et al.*, Org. Electron., **12** (2011) 566-574.
[4] J-W Kang *et al.*, Sol. Energy Mater. Sol. Cells, **103** (2012) 76-79.
[5] Bo. Nilsson *et al.*, Radiotherapy and Oncology, **11** (1988) 279-288.
[6] D. Menichelli *et al.*, Nucl. Instr. and Meth., A **583** (2007) 109-113.
[7] M. Grätzel, Inorg. Chem., **44** (2005) 6841-6851.
[8] Ahmed El-Zohry *et al.*, J. Phys. Chem., **116** (2012) 26144-26153.

CO4-11   Tritium Release from Li$_4$SiO$_4$ Ceramic Breeder Materials Prepared by Melt-Spraying Method

K. Munakata, K. Wada, A. Nakamura and T. Takeishi[1]

Department Faculty of Engineering and Resource Science, Akita University
[1]Graduate School of Engineering Science, Kyushu University

INTRODUCTION: Tritium release from new-types of Li$_4$SiO$_4$ ceramic breeder material was investigated. The Li$_4$SiO$_4$ breeder materials were prepared by the fabrication process called melt-spraying method. Tritium release curves were obtained in a series of experiments carried out using the out-of-pile temperature programmed desorption (TPD) technique. Tritium release curves obtained for solid breeders were compared.

EXPERIMENTS: The Li$_4$SiO$_4$ ceramic breeder materials (KALOS31 and KALOS34C) were prepared and supplied by Karlsruhe Institute of Technology (KIT). These ceramic breeders encapsulated in a quartz tube were irradiated in Kyoto University Research Reactor (KUR) in the thermal neutron with the flux of 5. 5×10^{12} cm^{-2}s^{-1} in the He atmosphere for 30 min.

Release curves of bred tritium from the breeder pebbles were obtained using the out-of-pile temperature programmed desorption techniques. The experimental apparatus is schematically shown in Figure 1. The volumes of ionization chambers are 66 cc, which corresponds to residence time, the chambers [volume] / [flow rate], 40 seconds. The first ionization chamber was used to measure the total tritium (HT and HTO) concentration and the second chamber placed after a water bubbler was used to measure that of molecular form tritium (HT) in the purge gas, respectively.

Water vapor was introduced to the purge gas just before the inlet of the first ionization chamber in order to minimize the memory effects on the ionization chambers. Dry argon gas or argon gas containing hydrogen was used as the sweep gas to investigate the effect of difference in sweep gas compositions.

RESULTS: Figure 2 shows comparison of experimental tritium release curves for the Li$_4$SiO$_4$ sample (KALOS31 and KALOS34C) irradiated for 30 minutes with neutron flux with 5. 5×10^{12} cm^{-2}s^{-1} [1/cm^{2}s]. The sweep gases of 1,000 ppm H$_2$/Ar gas were used in the experiments. Peak tritium concentrations were observed at 400 K for KALOS31, whereas it was observed at 800 K for KALOS34C, Comparison of Figs. 2(a) and (b) indicates that tritium was released at lower temperatures from the KALOS31 breeder material.
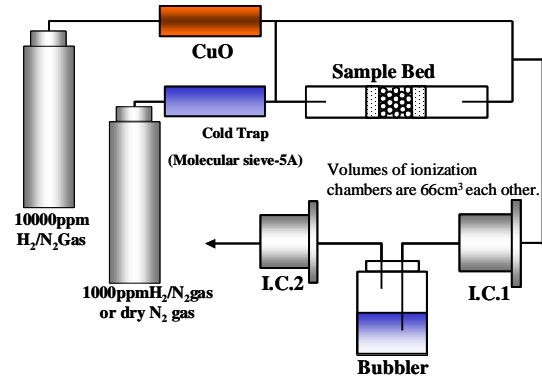

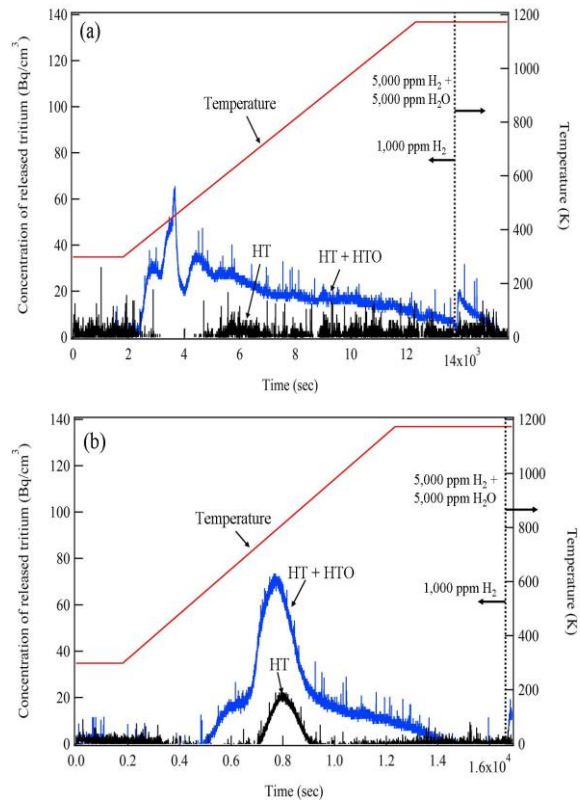**Fig.1** Schematic diagram of experimental apparatus

Fig. 2 Tritium release curves
(a) KALOS31 Li$_4$SiO$_4$ ceramic breeder material
(b) KALOS34C Li$_4$SiO$_4$ ceramic breeder material

CO4-12   **Polarization Degree of Linearly Polarized Coherent Transition Radiation Emitted from Wire-Grid Radiators**

T. Takahashi

Research Reactor Institute, Kyoto University

INTRODUCTION: In recent years various types of coherent radiation emitted from a short bunch of relativistic electrons have attracted a considerable attention as a bright light source in the THz-wave and millimeter wave regions for the spectroscopic purpose. Coherent transition radiation (CTR), which is emitted from a boundary between two media, is one of such a coherent light source. The electric vector of transition radiation (TR) emitted from a metallic screen is axially symmetric with respect to the trajectory of an electron beam, whereas synchrotron radiation has linear polarization along an electron orbit. Therefore, CTR is usually utilized as a non-polarized light source in the present spectroscopic application. However, circularly polarized light has been useful in the circular dichroism spectroscopy. Shibata *et al*. has developed a technique of generation of circularly polarized millimeter-wave radiation with the phase difference between the forward TR and the backward one [1]. However, it was difficult to control the polarization degree in that technique. In my previous report [2] the property of CTR emitted from a pair of wire-grid radiators with the different polarization was experimentally investigated in order to develop a new technique of generation of circular polarized THz radiation. In this report the polarization degree has been experimentally investigated in order to confirm the purity of polarization.

EXPERIMENTAL PROCEDURES: The experiment was performed at the coherent radiation beamline [3] at the L-band linac of the Research Reactor Institute, Kyoto University. The energy, the width of the macro pulse, and the repetition rate of the electron beam were 42 MeV, 47 ns, and 60 Hz, respectively. The average current of the electron beam was 3 μA. The schematic arrangement of the experiment is shown in Fig. 1. As the radiator of forward and backward CTR, wire-grid polarizers 10 μm thick with 25 μm spacing were used, respectively. The direction of grid of the first polarizer was horizontal and that of the second one was vertical. The CTR was detected by a liquid-helium-cooled Si bolometer. In order to measure the polarization degree a wire-grid polarizer with a rotary holder was used in front of the detector.

RESULTS: The distance between the forward and backward radiators is usually called the emission length. The polarization degree was calculated using the horizontal component (I_H) and the vertical one (I_V) of observed CTR intensity as

$$P_L = \frac{I_V - I_H}{I_V + I_H} \ .$$

The results are shown in Table 1 with changing the emission length. The observed CTR was not perfectly polarized (P_L=1). The reason seems to be the stray light in the vacuum chamber. However, the decrease of polarization degree is not affected to the development of the circular polarization because the rate of the stray light is very low and the observed polarization degree was independent of the emission length.

REFERENCES:

[1] Y. Shibata *et al.*, Rev. Sci. Instrum. **72** (2001) 3221.
[2] T. Takahashi, *et al.*, KURRI-PR 2012 CO4-15.
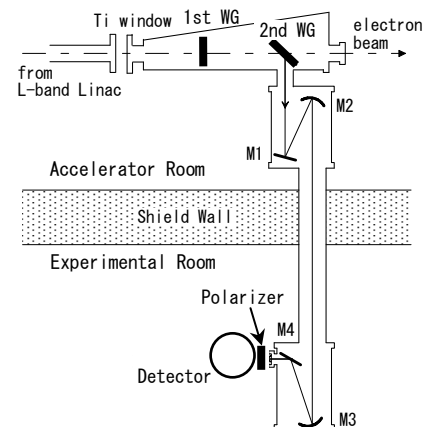[3] T. Takahashi *et al.*, Rev. Sci. Instrum. **69** (1998) 3770.

Fig.1. The schematic layout of the experiment.

Table 1. The polarization degree of observed CTR.

Emission Length	Polarization Degree
200 mm	0.85
500 mm	0.86
780 mm	0.86

CO4-13   **Effects of High Energy Particle Irradiation on Hydrogen Retention in Refractory Metals**

K. Tokunaga, M. Matsuyama[1], S. Abe[1], S. Nagata[2],
B. Tsuchiya[3], M. Tokitani[4], H. Osaki[5], K. Araki,
T. Fujiwara, M. Hasegawa, K. Nakamura, K. Hanada,
H. Zushi, Q. Xu[6] and K. Sato[6]

Research Institute for Applied Mechanics, Kyushu University
[1]*Hydrogen Isotope Research Center, University of Toyama*
[2]*Institute for Materials Research, Tohoku University*
[3]*Faculty of Science and Technology, Meijo University*
[4]*National Institute for Fusion Science*
[5]*Interdisciplinary Graduate School of Engineering Sciences, Kyushu University*
[6]*Research Reactor Institute, Kyoto University*

INTRODUCTION: It is of importance to clarify phenomena of implantation, retention, diffusion and permeation of tritium on surface of the armor materials of the first wall/blanket and the divertor on fusion device from a viewpoint of precise control of fuel particles, reduction of tritium inventory and safe waste management of materials contaminated with tritium. Refractory metals such as tungsten is potential candidate for an armor of the first wall and the divertor plate of the fusion reactor because of its low erosion yield and good thermal properties. The armor material will be subjected to heavy thermal loads in the steady state or transient mode combined with high energy neutron irradiation that will cause serious material degradation. In addition, high energy runaway electrons would bombard the armor materials along the equatorial plane in fusion device. It is considered that these cause radiation damage and enhance tritium retention. In the present works, tritium exposure experiments have been carried out for long term installed samples on a high temperature plasma experimental device. In addition, high energy electrons irradiation has been carried out to investigate effects of high energy electrons irradiation on tritium retention of tungsten using LINAC in Research Reactor Institute, Kyoto University.

EXPERIMENTS: Samples have been installed on vacuum chamber of spherical tokamak QUEST in Kyushu University. The vacuum vessel, and an armor of divertor and center stack of QUEST are made of SUS316L and tungsten, respectively. After the plasma discharge experiments, the samples have been examined using XPS, RBS and ERD. In addition, tritium exposure experiments have been carried out using a tritium (T) exposure device in University of Toyama. Pressure of the T gas was 1.3 kPa and T exposure was kept for 4 h in all examinations. T concentration in the gas was about 5 %. After thermal exposure to T gas, T amount retained in surface layers of the sample was evaluated by β-ray-induced X-ray spectrometry (BIXS) and imaging plate (IP) measurements.

RESULTS: Results from XPS analyses on the SUS316L sample which was installed in the 3rd cycle (from 2009/11 to 2010/4) showed that re-deposited layer was formed and main composition was C. BIXS neasurement which temperatures of pre-heating and T exposures were 400 ^{o}C and 350 ^{o}C, respectively showed that Fe(K_{α}) etc. peaks originated from composition of SUS6316L in addition to Ar(K_{α}) peak, originated from β ray on T near surface of SUS316L, were detected. IP measurement indicated that amount of T on the re-deposied sample at RT and 350 ^{o}C exposure was 4.6 and 2.5 times higher that that of non-exposure sample in QUEST. On the other hand, re-deposited layer, which main composition was Fe, Cr, W and O, was formed on SUS316L sample which was installed in the 7 th cycle (from 2011/10 to 2012/4). Amount of T on the re-deposited sample which temperatures of pre-heating and T exposures were both 100 ^{o}C (same temperature of wall during plasma discharge experiment in QUEST) was 8.5 times higher tthat of non-exposure sample in QUEST. In addition, results from T exposure experiment is summarized in Fig. 1. These results indicate that formation on re-deposited layer enhances T retention, and amount of T must be evaluated taking into account the re-deposited layer. In addition, high energy electrons with 10 MeV have been irradiated on two kinds of tungsten samples using LINAC in Research Reactor Institute, Kyoto University. Total fluence of electron was 4.6 x 10^{23} /m^2. Tritium exposure experiment will be carried out next fiscal year.
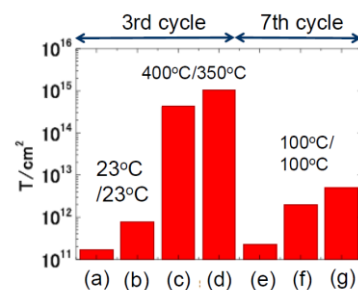

Fig. 1. Amount of T retention of various sample.
(a) Plasma un-exposed sample, pre-heating:23°C, and T exposure : 23°C.
(b) 3rd plasma exposed sample, pre-heating:23°C, T exposure : 23°C.
(c) Plasma un-exposed sample, pre-heating:400°C, and T exposure:350°C.
(d) 3rd plasma exposed sample, pre-heating:400°C, T exposure : 350°C.
(e) Plasma un-exposed sample, pre-heating:100°C, and T exposure : 23°C.
(f) 7th plasma exposed sample, pre-heating:100°C, T exposure : 100°C.
(g) 7th plasma exposed sample after sputtering, pre-heating:100°C, T exposure : 100°C.

CO4-14

γ-Ray Irradiation Effects for Various Metal Complexes with Cage-Type Silsesquioxane

Y. Okaue, T. Yokoyama, H. Ohashi[1] and F. Yoshimura

Department of Chemistry, Faculty of Sciences, Kyushu University
[1]Faculty of Arts and Science, Kyushu University

INTRODUCTION: Upon ^{60}Co γ-ray irradiation at room temperature on Q_8M_8 ($[(CH_3)_3SiO]_8(SiO_{1.5})_8$) with a double four-ring (D4R) cage structure as illustrated in Fig. 1, hydrogen atom is encapsulated in the D4R cage and is stable for periods of several years. The encapsulation of hydrogen atom can be confirmed by ESR spectroscopy. Hydrogen atom encapsulated in D4R cage of silsesquioxane interacts magnetically with paramagnetic oxygen molecules outside D4R cage to change ESR signal intensity and saturation behavior[1]. The purpose of this study was the preliminary research for interactions between metal ions and encapsulated hydrogen atom within single molecule by introducing coordination sites for metal ion to silsesquioxane with D4R cage structure. In this study, Schiff base ligand (L1 in Fig. 1) was prepared by condensation of $T_8{}^iBu_7Ap$ and salicylaldehyde.

Q_8M_8 ; R_1, R_2 = $OSi(CH_3)_3$

$T_8{}^iBu_7Ap$; R_1 = $CH_2CH(CH_3)_2$
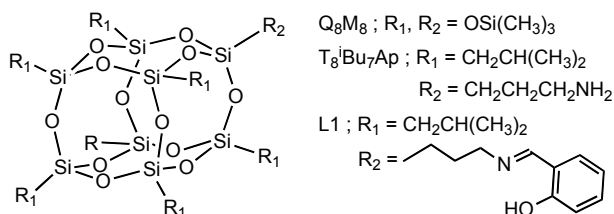R_2 = $CH_2CH_2CH_2NH_2$

L1 ; R_1 = $CH_2CH(CH_3)_2$

Fig. 1. D4R cage structure of silsesquioxane.

EXPERIMENTS: Various metal complexes of L1 were synthesized as follows: In the presence of excess triethylamine, metal acetate (Mn(II), Co(II), Ni(II), Cu(II), Zn(II)) and L1 were stirred in methanol at 60 °C for 2 h. The resulting solution was concentrated under reduced pressure and cooled to room temperature. Powder with characteristic color for the aimed metal complex was obtained. In the case of oxovanadium(IV) complex, oxovanadium(IV) sulfate was used as metal source instead of metal acetate. Characterizations were made by IR spectroscopy, ^{1}H NMR spectroscopy, and elemental analyses. Powder samples of metal complexes were irradiated with γ-ray under air at room temperature in ^{60}Co γ-Ray Irradiation Facility at Kyoto University Research Reactor Institute. Irradiated samples were recrystallized from hexane. X-band ESR spectra for the recrystallized powder samples under air or nitrogen atmosphere were measured on JEOL JES-FA200 spectrometer at room temperature.

RESULTS: All metal complexes were obtained as

$M(L1)_2$ (M = V(IV)O, Mn(II), Co(II), Ni(II), Cu(II), Zn(II)). The colors and yields for these metal complexes were listed in Table 1.

Table 1. Colors and yields for $M(L1)_2$

Metal	Color	Yield / %
V(IV)O	green white	54
Mn(II)	brown	70
Co(II)	yellow	68
Ni(II)	light green	79
Cu(II)	dark green	77
Zn(II)	yellowish white	54

ESR spectra of all metal complexes showed the characteristic two hyperfine lines separated with about 50 mT due to hydrogen atom nucleus attributed to the encapsulated hydrogen atom in the D4R cage of silsesquioxane unit. For example, ESR spectrum of the irradiated $Ni(L1)_2$ was shown in Fig. 2. In the case of ESR spectrum for the irradiated $VO(L1)_2$ or $Cu(L1)_2$, typical spectral pattern due to metal ion (V(IV) or Cu(II)) was shown and the signals for the encapsulated hydrogen atom were very small. Under nitrogen atmosphere, ESR signals due to the encapsulated hydrogen atom were observed for the irradiated metal complexes except $VO(L1)_2$ and $Cu(L1)_2$. In hexane solution, the signals due to the encapsulated hydrogen atom were also shown under air and nitrogen atmosphere for the irradiated metal complexes except $VO(L1)_2$ and $Cu(L1)_2$.

From these results, it was concluded that three types of interactions between metal ions and encapsulated hydrogen atom were observed: 1) Large interaction for paramagnetic $VO(L1)_2$ and $Cu(L1)_2$, 2) Small interaction for paramagnetic $Mn(L1)_2$ and $Co(L1)_2$, 3) No interaction for diamagnetic $Ni(L1)_2$ and $Zn(L1)_2$.
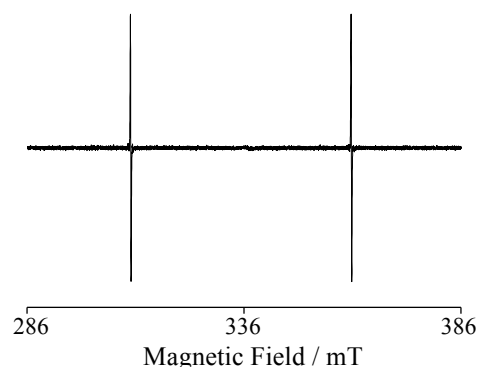

Fig. 2. ESR spectrum of irradiated $Ni(L1)_2$.

REFERENCE:
[1] R. Sasamori, Y. Okaue, T. Isobe and Y. Matsuda, Science, **265** (1994) 1691-1694.

Dependence of Irradiation Damage Density on Tritium Migration Behaviors in Li$_2$TiO$_3$

K. Okuno, Y. Oya, M. Kobayashi, H. Uchimura, K. Toda, M. Sato, T. Fujii[1] and H. Yamana[1]

Graduate School of Science, Shizuoka University
[1]Research Reactor Institute, Kyoto University

INTRODUCTION:

For the development of D-T fusion reactors, it is important to establish an effective fuel recycling system and a comprehensive model of tritium (T) migration processes in solid T breeding materials. In the test blanket module for ITER, lithium titanate (Li$_2$TiO$_3$) is thought to be one of candidates as T breeding materials. T trapping/detrapping by irradiation damages would make a large influence on T migration with increasing neutron fluence. In this study, T release behavior for Li$_2$TiO$_3$ with various neutron fluences were studied by means of Thermal Desorption Spectroscopy (TDS). The effect of purge gas condition was also examined to demonstrate the actual tritium recovery environment in fusion reactor.

EXPERIMENTAL:

Powder of Li$_2$TiO$_3$ purchased from Kaken Co. was used as samples. The Pn-2 was used to irradiate by thermal neutron with the fluence of 3.3 x 10^{14} (sample A), 3.3 x 10^{15} (sample B), 1.7 x 10^{16} (sample C), 3.3 x 10^{16} (sample D) n cm^{-2} at the Kyoto University Research Reactor Institute (KURRI). The other samples were introduced into the inner side of reactor, namely the core region of reactor for higher neutron fluence (Long Irradiation, LI), where the neutron fluence was 2.2×10^{19} n cm^{-2} (sample E). After neutron irradiation, the density of irradiation damages introduced in Li$_2$TiO$_3$ by neutron irradiation, was measured by Electron Spin Resonance (ESR) at liquid nitrogen temperature. Out-of-pile T release experiments were performed in T-TDS system at Shizuoka University.

RESULTS&DISCUSSION:

The irradiation damages of F$^+$-centers and O$^-$-centers were formed by neutron irradiation, and their damage densities were increased with increasing neutron fluence. T release temperature was clearly shifted toward higher temperature side with increasing neutron fluence, i.e. increasing damage density. The rate determining process for tritium release was clearly changed, depending on the damage density. T release

was mainly controlled by T diffusion process in crystalline grain of Li$_2$TiO$_3$ at lower neutron fluence. The apparent T diffusivity was reduced as the damage density in Li$_2$TiO$_3$ increased due to the introduction of T trapping/detrapping sites for diffusing T. Therefore, T trapping/detrapping processes began to control the overall T release with further damage introductions as the amount of T trapping sites increased enough to trap most of T in Li$_2$TiO$_3$. The kinetics analysis of T release for highly damaged Li$_2$TiO$_3$ showed that the rate determining process of T release was the detrapping process of T formed as hydroxyl groups. The rate of T detrapping as hydroxyl groups was determined by the kinetic analysis, and was comparable to T release kinetics for Li$_2$O, LiOH and Li$_4$TiO$_4$. The dangling oxygen atoms (O$^-$-centers) formed by neutron irradiation would strongly contribute on the formation of hydroxyl groups. The efficiency of T trapping/detrapping by the dangling oxygen atoms was clearly increased with increasing damage density due to the stabilization of damages by neighboring irradiation damages and/or the lithium burn-up which produces lithium vacancy acting as a pass way of T to the dangling oxygen atoms.
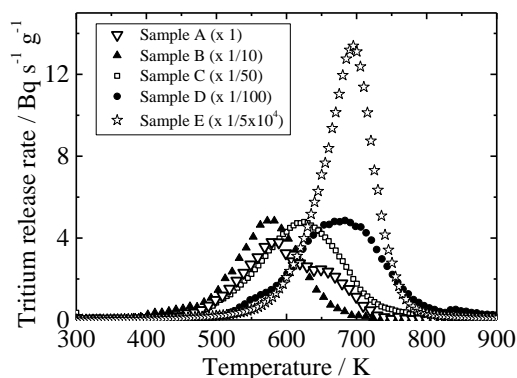

Fig. T-TDS spectra for Li$_2$TiO$_3$
with various neutron fluences

Complex Structure of Ions Coordinated with Hydrophilic Polymer. 14.

A. Kawaguchi , Y. Gotoh[1] and Y. Morimoto

Research Reactor Institute, Kyoto University
[1]*Faculty of Text. Sci. and Tech., Shinshu Univ.*

INTRODUCTION: We have reported composite structure brought by *in situ* preparation through "secondary doping" by diffusion of metallic ions into iodine-doped hydrophilic polymers. Polyiodide ions, I_n^{m-} (*m, n*: integer, $n \neq 1$), which have been as solutes in aqueous solution, can be doped into the polymers without modification of the matrixes. And, furthermore, the polymer matrix previously iodine-doped enhances following diffusion of other molecules or ions into matrix polymer; if the additional ion makes precipitates of inorganic salt with iodide, hybrid composite can be achieved without melting, nor casting, nor synthesizing.[1-3]
Such process for "iodine (first) doping" and for following "secondary (or more) doping" of additional ions can be achieved depending on diffusion of the ions into the resin matrixes. Then, ionic diffusion process without modification of macroscopic shapes of the samples means merits for arbitrariness of hybrid composite without plasticization; their shapes or (often) chain orientation are maintained in the composites in the final stage, and it provides preparation methods for hybridization of polymeric matrixes which can not be solved in solution nor be melt above T_m, such as natural materials [3].

EXPERIMENTS: Bamboo fiber (*phyllostachys heterocycla*, maybe) which had grown naturally in ground of KURRI (Kumatori, Osaka, JAPAN) was prepared as starting matrix for doping. A branch of bamboo was manually crushed and cut to short pieces (D:3-5mm x L:15-20mm). The divided pieces were immersed in methanol (for 1 week, at R.T.) to reduce impurities and, next, were aged in vacuum in a heater at 150°C for 2 weeks.
Iodine doping was achieved with I_2-KI(aq)/0.8N (for 2 months, at R.T.) and secondary doping was done with $AgNO_3$(aq)/1M (for 78 hrs., at R.T.). Electric conduction was measured with DMM as "two probe method". Some samples were observed with wide-angle X-ray diffraction (WAXD) by MoKα incident.

RESULTS AND DISCUSSION: Generally, main component as polymeric fiber in the bamboo sample is cellulose (phase-I) which is not soluble in water nor methanol at R.T. [4] Neither our "iodine doping" showed degradation of fiber in the samples, as macroscopic shapes and diffraction with X-rays. (Fig.)
On the other hand, iodine doping process colored the samples dark brown or black explicitly and increase in

mass (Δm) on iodine doping was c.a. 50-90%. And, on following "secondary doping" with Ag^+ ion, the samples were colored gray and Δm was c.a. 100-140% after immersing them into $AgNO_3$(aq).(Fig.(a)) Further, electric conductivity showed anisotropy for fiber axis. For example, DC resistance parallel to a sample of bamboo fiber was 5-10MΩ against 15-25MΩ for one normal to the axis; as conductivity, the former parallel to fiber axis was several times or tenfold larger than latter normal to it.(Fig.(a)) However, considering behavior on each process, situation in micro structure of the bamboo fiber was different from hydrophilic polymers previously reported such as polyamide-6 (PA6); while slight anisotropy of AgI precipitates as inorganic fillers was observed for fiber axis, no explicit modification of cellulose crystallites or its chain orientation as host matrix was observed on "iodine doping" nor on "Ag secondary doping".[5]
These results is regarded as deep permeation of polyiodide ions and following precipitation of AgI salt, which is also accepted with WAXD pattern. Non-negligible amount of AgI precipitates explicitly exist in the bamboo composite(Fig.(c)), but, in the case of the bamboo matrix, polyiodide ions are considered to induce ionic diffusion into intermediate region among cellulose crystallites. Consequently, even if the samples had not indicated explicit precipitation of AgI after "Ag secondary doping" in microscopic appearance, traffic of iodine or metal ions (and precipitation of AgI salt) might not advance at cellulose crystallites.

Fig. Macroscopic appearance(a: left), optical microscope image (b: center, x40) and WAXD pattern (c: right) of bamboo matrix prepared by "secondary doping" with Ag^+ following "iodine doping".

REFERENCES:
[1] A. Kawaguchi, Sens. Actuators B, **73** (2001) 174-178.
[2] Y. Gotoh, *et.al.*, Polym. Prep. Jpn., **51** (2002), 2259-2259.
[3] patent. JPN-5444559 (2014).
[4] "Sen'i-Bin'ran", 3rd ed., ch.1 (in Japanese, Ed. by Soc. Fiber Sci. Tech, Jpn., Maruzen, 2004).
[5] A. Kawaguchi, *et.al.*, Polym. Prep. Jpn., **52** (2003), 577-577.

CO4-17　　　Thermoresponsive Porous Binary Gels Prepared through γ-Irradiation

N. Sato, Y. Oba, R. Inoue and M. Sugiyama

Research Reactor Institute, Kyoto University

INTRODUCTION: Polymer gels are known to consist of the three-dimensional network of crosslinking polymer chains. These network can contain a large amount of liquids, especially water in the most cases, within its structure while keeping its solid form. This unique property contributes to the biocompatibility of polymer gels, and therefore they are widely used for medical, hygiene, food products like diapers, contact lenses, wound dressing, and food additives. The various properties of gels such as swelling, mechanical strength and elasticity are strongly dependent on its network structure, which have been attracting scientific interest of researchers in various fields. The quality and function of polymer gels can be further improved by understanding a variety of factors which affect the molecular structure of the gels: crosslink density, physical and chemical nature of component polymer chains, electronic charges, and structural imhomogeneities.

The most common method for gel preparation is chemical crosslinking. Typically, polyfunctional monomers are mixed together with monofunctional monomers and then polymerized together to form crosslinking polymer network. Crosslink density can be controlled by changing the concentration of the polyfunctional monomers. Radiation-induced gel preparation method is another well-employed technique to prepare polymer gels. In this method, gels can be synthesized only by irradiating γ-rays to polymer solutions and no chemical crosslinkers or reaction initiators are required. Crosslink density can be controlled by the concentration of the polymer solution and the condition of γ-irradiation. In comparison with chemical-crosslinking gels, radiation-crosslinking gels have advantages in reduced impurities remaining in the final product gels as well as more homogeneous structure of three-dimensional network. Thus radiation-crosslinking gels have potential to show quality superior to chemical-crosslinking gels.

Another merit of radiation preparation of polymer gels is the easy preparation of gels with special structure. We have already succeeded in preparing porous gels and multicomponent gels by simple procedures including γ-irradiation. It is expected to be applicable to other designed structure of polymer gels aiming at intelligent gel materials.

In this report, we describe the radiation preparation of nonporous and porous hydrogels composed of two different classes of polymers: poly(ethylene glycol) (PEG) and poly(N-isopropylacrylamide) (PNIPAm). The former is known as a common hydrogel polymer; the latter as a typical thermoresponsive polymer whose gels show volume transition around 34°C. Another report of ours addresses microscopic structure of these gels as revealed by small-angle scattering measurement. This report deals with details of synthesis and macroscopic changes of swelling status on temperature change.

EXPERIMENTS: PEG/PNIPAm binary porous gels were prepared by the following procedures. Silica microparticles (200 and 1000 nm in diameter) were mixed with a PEG aqueous solution (10 wt%) under ultrasonic irradiation followed by N_2 bubbling for deoxygenation. After sealed in a glass vial, the solution was irradiated with γ-rays for 60 kGy at a dose rate of 1.0 kGy/h at Co-60 Gamma-ray Irradiation Facility of Research Reactor Institute, Kyoto University. The silica microparticles in the crude gel were decomposed with 20% hydrofluoric acid for 24 h, and then fully washed with water. The PEG matrix gels thus obtained were immersed in a NIPAm monomer aqueous solution (10 wt%) and irradiated with γ-rays again for 3 kGy at a dose rate of 1.0 kGy/h. Unreacted monomers were washed out by rinsing with water after irradiation, and purified product gels were finally obtained.

RESULTS AND DISCUSSION: Incorporation of PNIPAm chains into PEG matrix gels by γ-irradiation was confirmed from IR spectra as shown in Fig. 1. After irradiation of γ-rays to a PNIPAm-impregnated gel, a new absorption peak appeared around 1700 cm^{-1}, which can be assigned to C=O stretching for the carbonyl group.

PEG/PNIPAm binary gels swollen in cold water shrunk when the temperature was raised to 40 °C. This result proves that thermoresponsive property was inherited by the binary gels from γ-ray induced preparation. The degree of the shrinkage for the porous gel was lower than that for the nonporous gels. This indicates that PNIPAm chains were highly localized in the pore space.
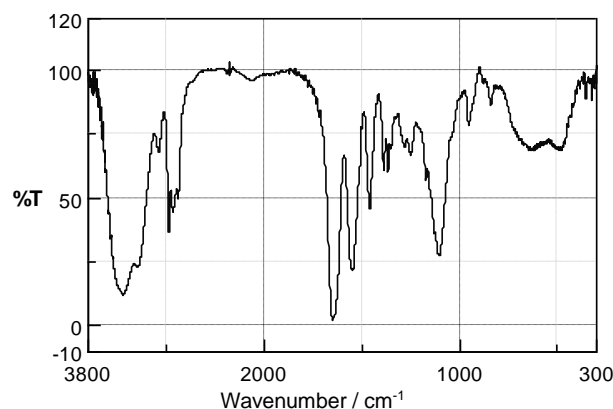
Fig. 1. IR spectrum of a nonporous PEG/PNIPAm binary gel. Absorption of the carbonyl group found around 1700 cm^{-1} is a proof of incorporation of PNIPAm chains.

CO4-18   Design and Preparation of the Electrochemical Cell for the Study of the Electrical Double Layer at the Electrochemical Interfaces of Ionic Liquids Using Neutron Reflectometry

N. Nishi, Y. Ikeda and M. Hino[1]

Graduate School of Engineering, Kyoto University
[1]Research Reactor Institute, Kyoto University

INTRODUCTION: Ionic liquids (ILs), which are liquid salts entirely composed of cations and anions, have potential applications to electrochemical devices because of their several characteristics such as negligible volatility and wide potential window at the IL/electrode interface. The knowledge of the molecular-level structure at IL/electrode interface is important to optimize the performance of the IL electrochemical devices. Theoretical studies have revealed several unique features of the distribution of ions at IL/electrode interface, such as over-screening effect and lattice-saturation effect, while experimental studies that shed light on such features are limited to a few. In this study, we aimed to investigate the electrical double layer at the IL/electrode interface using neutron reflectometry. In this report, we will show the results of the design and the preparation of the cell, which is crucial for sensitive detection of the ion distribution in the electrical double layer.

EXPERIMENTS: Thin-layer Al_4Ti, as a film electrode, was prepared on a silicon wafer using a sputter apparatus. For IL, trioctylmethylammonium bis(trifluoromethane-sulfonyl)amide ($[TOMA^+][C_1C_1N^-]$) was prepared from the hydrophilic salts of the IL-constituent ions ($[TOMA^+]Cl^-$ and $Li^+[C_1C_1N^-]$). Another IL, $[DEME^+][C_1C_1N^-]$ ($DEME^+$: diethyl-2-methoxyethylmethylammonium), was purchased. The two ILs were purified using column chromatography. Cyclic voltammograms were recorded at the film/IL/film two-electrode electrochemical cell.
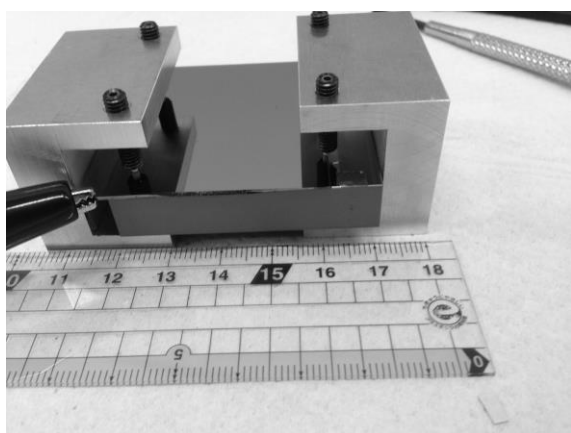

Fig. 1. Electrochemical cell for neutron reflectivity measurements.

RESULTS: Figure 1 shows the electrochemical cell designed and prepared for neutron reflectometry. IL was sandwiched with two Al_4Ti electrode films that were sputtered on the surface of silicon wafers. The surface of the bottom silicon wafer was polished and the surface roughness evaluated using x-ray reflectometry was ~3 Å. The interface between IL and the Al_4Ti electrode film on this polished silicon surface (bottom interface) will be "target" interface in neutron reflectometry. The bottom silicon wafer is thick, with a thickness of 1 cm, to shine the neutron beam from the edge of the wafer. The surface of the upper silicon wafer was non-polished because we do not want to see reflected beam from this surface and thus want to minimize and neglect the reflectivity from this surface. To prevent short circuit of the cell due to unintended contact of the two electrodes, thin layer glass sheet with a thickness of 50 μm was inserted as a spacer between the two electrodes. The area of the electrode was 30×50 mm^2 in order to keep the sufficient area to cover a long footprint of neutron beam with a grazing incident angle.

We tested the electrochemical polarizability of the cell using cyclic voltammetry. Figure 2 shows the cyclic voltammogram with a scan rate of 0.1 V s^{-1}. One can see electrochemical window over 1 V available for the cell depending on the IL, which indicates that we can perform neutron reflectivity measurements of the interfacial structure at various electrode potentials within the electrochemical window.
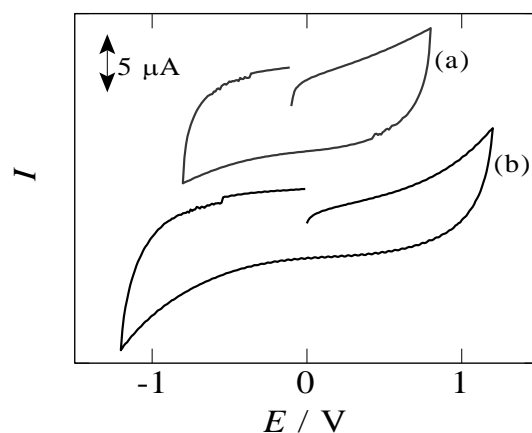

Fig. 2. Cyclic voltammogram for the electrochemical cell shown in Fig.1. Scan rate: 0.1 V s^{-1}; electrode surface area: 15 cm^2; ionic liquid layer spacing: 50 μm. IL: (a) $[TOMA^+][C_1C_1N^-]$ and (b) $[DEME^+][C_1C_1N^-]$ containing 1 mol/kg $Li^+[C_1C_1N^-]$.

^{57}Fe Mössbauer Study of a Reactive Diiron Paddlewheel Unit in a Porous Coordination Polymer

K. Kongpatpanich[1], S. Horike[1,2], M. Sugimoto[1], S. Kitao[3], M. Seto[3] and S. Kitagawa[1,4]

Graduate School of Engineering, Kyoto University
[1]*Department of Synthetic Chemistry and Biological Chemistry, Kyoto University*
[2]*Japan Science and Technology Agency, PRESTO*
[3]*Research Reactor Institute, Kyoto University*
[4]*Institute for Integrated Cell-Material Science (iCeMS), Kyoto University*

INTRODUCTION: Porous coordination polymer (PCP) has been broadly studied for its adsorptive functions [1,2]. One of the current challenges in this area is the incorporation of the reactive metal unit into the structure. Dirron paddlewheel unit, $[Fe_2(\mu\text{-}O_2C\text{-}R)_4]$, is redox-reactive due to the variable chemical state of the two iron ions in the unit. In this work, we synthesized porous coordination polymer containing the diiron paddlewheel unit, $[Fe_2(1,4\text{-}BDC)_2(dabco)]\cdot(1)$, and studied on the chemical state of iron by using ^{57}Fe Mössbauer spectroscopy.

EXPERIMENTS: Due to the air-sensitive nature of a sample, we prepared the sample as a pallet in an Ar-filled glovebox. ^{57}Fe Mossbauer spectroscopy was performed under dynamic vacuum by using a ^{57}Co source with a nominal activity of 1.85 GBq. Velocity scale was calibrated as isomer shifts relative to α-Fe foil. Initial parameters for the least-square of 1 obtained from fitted parameters of the air-exposed sample of 1. All measurements were carried out at 77 K and the measurements were repeated at 150 K.

RESULTS: $[Fe_2(1,4\text{-}BDC)_2(dabco)]\cdot(1)$ is air-sensitive as noticeable from its color change, suggesting the transformation *via* redox reaction. We measured ^{57}Fe Mössbauer spectra of 1 before and after air-exposure to investigate on the oxidation state of Fe ions in the sample. The spectrum of 1 collected at 77 K (Fig. 1) is fitted into two quadrupole-split doublet signals, which are characteristic of high-spin Fe^{2+} and Fe^{3+}. The relative absorption areas of the two subspectra correspond to 91.6% of Fe^{2+} and 8.4% of Fe^{3+}. Mössbauer spectroscopy of the same sample was measured again at 150 K to confirm the reliability of the least-square fitting and the peak assignment. The dominant doublet with isomer shift value at 1.25 mms^{-1} and quadrupole-splitting value of 2.72 mms^{-1} is typical for high-spin Fe^{2+}. It is determined that the compound contains diiron paddlewheel unit in +2 oxidation state from the characteristic doublet peak in the Möss-

bauer spectrum. On the other hand, the other minor doublet signal with isomer shift at 0.56 mms^{-1} and quadrupole-splitting value of 0.90 mms^{-1} corresponds to high-spin Fe^{3+} species. It is supposed that Fe^{3+} ions come from the air-contamination in 1 occurred during sample transfer for the measurement of the Mössbauer effect, because of the high reactivity of 1 to the air. We oxidized 1 by air-exposure for 12 hours at 298 K and measured Mössbauer spectrum. As expected, Mössbauer spectrum of the air-exposed sample dominantly shows doublet of high-spin Fe^{3+} (92.4% of relative peak area) from the framework oxidation along with the collapse of the framework. This indicates water molecules in air would replace ligands in 1 and subsequently Fe^{2+} ions in the paddlewheel unit are oxidized to Fe^{3+}.
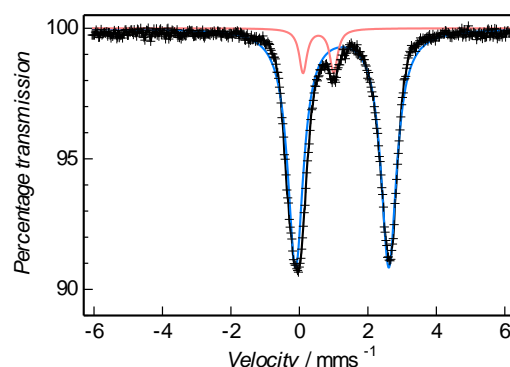

Fig. 1. ^{57}Fe Mössbauer spectrum of 1 measured at 77 K. The wide doublet corresponds to high-spin Fe^{2+}, while the narrow doublet is assigned to high-spin Fe^{3+} [3].

REFERENCES:
[1] O. M. Yaghi *et al.*, Nature, **423** (2003) 705-714.
[2] S. Kitagawa *et al.*, Angew Chem. Int. Ed., **43** (2004) 2334-2375.
[3] K. Kongpatpanich *et al.*, Chem. Commun., **50** (2014) 2292-2294.

[129]I Mössbauer Spectroscopy of Silver Iodide Quantum Dots

T. Yamamoto, K. Otsubo, H. Kitagawa, S. Kitao[1] and M. Seto[1]

Graduate School of Science, Kyoto University
[1]Research Reactor Institute, Kyoto University

INTRODUCTION: Nanomaterials have been extensively studied in the fields of science and technology due to their unique properties arising from high surface area-to-volume ratios and quantum size effects. Silver iodide (AgI) has been used as photosensitizers and for cloud seeding. AgI is also a superionic Ag^+ conductor in the high-temperature α-phase, and has been studied as a solid electrolyte for solid-state batteries[1]. In addition, AgI is a direct bandgap semiconductor in the low-temperature β- and γ-phases, and its optical properties have been investigated in both bulk and nanomaterials.

There are a variety of methods to synthesize AgI nanoparticles, for example AgI nanoparticles in glass matrix were fabricated by a quenching technique from high temperature over 500 °C[2]. Polymer-based liquid-phase techniques have also been adopted as facile and effective methods for the preparation of size-controlled AgI nanoparticles[3]. Although AgI nanoparticles in the size range of 4 - 41 nm have been obtained as a solid phase and well characterized so far[4-6], the development of a facile synthetic method for AgI quantum dots smaller than 4 nm is still required. Very recently, we have reported a facile low-temperature liquid-phase synthesis method of small AgI quantum dots with a diameter of 3.0 nm[7]. Here we report [129]I Mössbauer spectroscopy of AgI quantum dots to investigate their electric states.

EXPERIMENTS: The AgI quantum dots were prepared by a liquid-phase method. In order to avoid photoreduction of AgI, the synthesis was carried out with an apparatus covered with aluminum foil. $AgNO_3$ (0.067 mmol) and poly(*N*-vinyl-2-pyrrolidone) (PVP, 1.243 mmol) were dissolved in 60 mL of cold methanol and stirred for several minutes at the ice temperature. Then 3.4 mL of Na[129]I aqueous solution (1.61 µCi / mL) was added quickly and stirred for 2 h at the ice temperature. The synthesized quantum dots were collected by centrifugation and dried in air.

[129]I Mössbauer spectroscopy on the prepared AgI quantum dots was performed at 50 K. Mg_3[129m]TeO_6 was used as the γ-ray source, which was prepared by neutron irradiation of Mg_3[128]TeO_6. The source velocity was calibrated by using pure α-Fe as the control material.

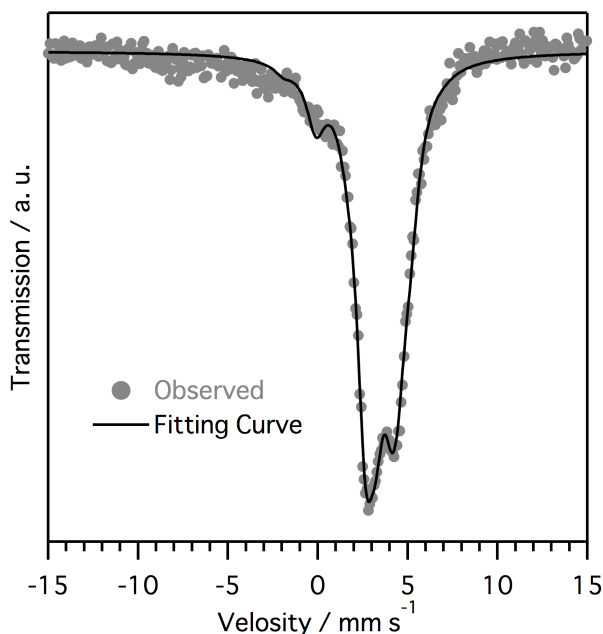**RESULTS:** The observed data (dots) and the fitting curve are shown in Fig. 1. The fitting gives the hyperfine

Fig. 1. The [129]I Mössbauer spectrum for AgI quantum dots using a Mg_3[129m]TeO_6 source at 50 K. The obtained hyperfine interaction parameters are IS = 3.30 mm/s, W = 1.23 mm/s, QCC = -408.5 MHz, and η = 0.21.

interaction parameters (isomer shift IS, line width W, quadrupole coupling constant QCC, and asymmetry parameter η). IS is 3.30 mm/s relative to the Mg_3[129m]TeO_6 source. The slightly large W value (1.23 mm/s) indicates that QCC has some distribution, and QCC is estimated at -408.5 MHz. Interestingly, the fitting gives better results with taking η as 0.21 rather than zero. From these parameters, it is supposed that the iodine in the AgI quantum dots has a charge slightly more positive than -1, although that in bulk AgI has -1. It is conceivable that this charge change derives from an interaction between the surface of the quantum dots and PVP.

REFERENCES:
[1] B. B. Owens, J. Power Sources, **90** (2000) 2-8.
[2] M. Tatsumisago, Y. Shinkuma and T. Minami, Nature, **354** (1991) 217-218.
[3] M. I. Vucemilović and O. I. Micić, Int. J. Radiat. Appl. Instrum., Part C, **32** (1988) 79-83.
[4] R. Makiura, T. Yonemura, T. Yamada, M. Yamauchi, R. Ikeda, H. Kitagawa, K. Kato and M. Takata, Nat. Mater., **8** (2009) 476-480.
[5] S. Yamasaki, T. Yamada, H. Kobayashi and H. Kitagawa, Chem. Asian J., **8** (2013) 73-75.
[6] B. Xu and X. Wang, Small, **7** (2011) 3439-3444.
[7] T. Yamamoto, H. Kobayashi and H. Kitagawa, Chem. Lett., DOI: 10.1246/cl.140409

CO4-21   Neutron Irradiation Effect of High-Density MoO₃ pellets for Mo-99 Production

K. Nishikata, T. Ishida, M. Yonekawa, Y. Kato,
M. Kurosawa, A. Kimura, Y. Matsui, K. Tsuchiya,
T. Sano[1], Y. Fujihara[1] and J. Zhang[1]

Neutron Irradiation and Testing Reactor Center, JAEA
[1]Research Reactor Institute, Kyoto University

INTRODUCTION: As one of effective applications of the Japan Materials Testing Reactor (JMTR), JAEA has a plan to produce ^{99}Mo by (n, γ) method ((n, γ)^{99}Mo production), a parent nuclide of ^{99m}Tc[1]. In this study, preliminary irradiation tests were carried out with the high-density MoO₃ pellets in the KUR and the ^{99}Mo production amount was evaluated between the calculation results and measurement results.

EXPERIMENTS: The high-density MoO₃ pellets were fabricated by the Plasma Sintering Method[2]. Theoretical Density (T.D.) of sintered MoO₃ pellets was targeted in a range from 90 to 97%. The high-density MoO₃ pellets were irradiated in the SLANT of KUR. Before the irradiation tests, neutron flux in the SLANT was measured with the dosimeters (In foil and In-Ni foil with Cd canning), and neutron spectrum and ^{99}Mo production amount was evaluated by MVP2.0 (Monte-Calro calculation cord) and JENDL-4.0 (nuclear data library). Table 1 shows the irradiation conditions of MoO₃ pellets in the SLANT of KUR. After the irradiation tests, the irradiated MoO₃ pellets were transported from KUR to JMTR-HL. The PIEs were carried out such as XRD analysis and SEM observation and the irradiated pellets were dissolved with 6M-NaOH solution in the Lead Cell.

RESULTS: Figures 1 show the neutron spectrum and ^{99}Mo production in the SLANT of KUR.

In this result, thermal neutron flux was about 3% bigger than KUR nominal value in this test. The total ^{99}Mo production amounts were $7.0×10^6$ Bq/g for 4 h and $3.3×10^7$ Bq/g for 24 h, respectively. From the PIE results by the XRD and SEM, it was found that no change of crystal structure and grain size was observed in the MoO₃ pellets irradiated at low temperature and fluence. The irradiated pellets could be dissolved sufficiently in 6M-NaOH solution within 3 h. After the dissolution of the irradiated MoO₃ pellets, radioactive nuclides were measured by the γ-ray spectrometer. Table 2 shows the results of ^{99}Mo production amounts. In this result, experimental values of ^{99}Mo were $9.0×10^6$ Bq/g for 4 h and $4.5×10^7$ Bq/g for 24 h, respectively, and measured values were almost the same as the calculated values.

CONCLUSION: As part of the development of the ^{99}Mo production by (n, γ) method, the high-density MoO₃ pellets were irradiated in the KUR and ^{99}Mo production amounts were currently evaluated by the neutron spectrum in the irradiation field and neutron capture cross-section of ^{98}Mo. In the PIEs, no change of crystal structure and grain size was observed in the MoO₃ pellets irradiated at low temperature and low fluence.

REFERENCES:
[1] K. Nishikata, et al., Fabrication and Characterization of High-Density MoO₃ Pellets, Proceedings of 2012 Powder Metallurgy World Congress & Exhibition (2012) CD-ROM.
[2] K. Tsuchiya, et al., Status of ^{99}Mo-^{99m}Tc Production Development by (n, γ) Reaction, JAEA-Conf 2011-003（2011）.

Table 1 Irradiation condition of MoO₃ pellets

Items	Values
Thermal power	1 MW
Irradiation hole	SLANT
Thermal flux	$1.8 × 10^{17}$ m^{-2}s^{-1}
Fast flux	$8.8 × 10^{16}$ m^{-2}s^{-1}
Irradiation Temp.	about 50 °C

Table 2 Results of ^{99}Mo production amounts

Irradiation Time (h)	^{99}Mo production amounts (Bq/g-MoO₃)		Measured value/ Calculated value
	Measured value	Calculated value	
4	$9.0 × 10^6$	$7.0 × 10^6$	1.3
24	$4.8 × 10^7$	$4.5 × 10^7$	1.1

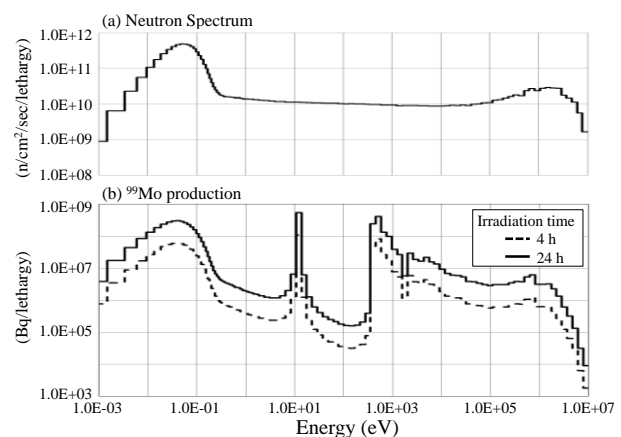Fig. 1 Neutron spectrum and ^{99}Mo production rate in the SLANT of KUR

CO4-22   Mössbauer Spectroscopy of Spinel Oxide Fe_2TiO_4 in Applied Magnetic Field

S. Nakamura, Y. Kobayashi[1], S. Kitao[1] and M. Seto[1]

Department of Science and Engineering, Teikyo University
[1]Research Reactor Institute, Kyoto University

INTRODUCTION: The ulvöspinel Fe_2TiO_4 has a cubic spinel structure (*Fd-3m*) with the lattice constants of *a*=8.5469Å at room temperature. The A-site is occupied by Fe^{2+} ion, whereas the B-site is occupied equally by Fe^{2+} and Ti^{4+} ions. The high spin Fe^{2+} ion on the tetrahedral site is a Jahn-Teller active ion and induces cubic-tetragonal phase transition at T_t =163K [1]. The low temperature tetragonal structure ($I4_1/amd$) has lattice constants of *a*=6.0129Å and *c*=8.5237Å at 123K, slightly elongated along the *c*-axis ($c/a\sqrt{2}$=1.0024). The magnetic structure is a Néel type antiferromagnet (T_N~130K) with a weak ferromagnetic moment along the *c*-axis [2, 3]. The Mössbauer spectrum of this compound consists of broad and complicated spectrum due to the B-site ion disorder and the domain structure below T_t [4]. In this research, we have conducted Mössbauer spectroscopy by using a single crystal specimen squeezed along [001] below T_t. As a result, a single domain state is realized and a better-resolved spectrum can be obtained.

EXPERIMENTS: The single crystal of Fe_2TiO_4 was prepared by FZ method in a controlled oxygen pressure. The (001) plane disk of about 6 mm diameter and 40μm thickness was used as an absorber. The edge of the disk was surrounded by epoxy resin. When the specimen was cooled through T_t, it was squeezed along the [001] direction and thus the tetragonal *c*-axis was specified. ^{57}Fe Mössbauer spectroscopy was conducted in conventional transmission geometry by using ^{57}Co-in-Rh (50mCi) as the γ ray source. The spectra were measured at *T*=15 K in applied magnetic field (H_{ex}) up to 14T. The directions of the γ ray and the magnetic field were both parallel to the tetragonal *c*-axis. The Doppler velocity was calibrated by using Fe metal foil. Lorentzian line shapes were assumed for the analysis.

RESULTS: In Fig.1, Mössbauer spectra of Fe_2TiO_4 at *T*=15 K in applied magnetic field are shown. We have analyzed the spectra by a four-subspectra model,

corresponding to two A-sites (A1 and A2) and two B-sites (B1 and B2), which is based on the local arrangement of the B-site ions [4]. At H_{ex}=0 T, the hyperfine fields (H_{hf}) are 33.9, 28.7, 28.7, and 22.2 T, respectively. Due to the local B-site arrangement, the principal axes of electric field gradient (EFG) of each Fe^{2+} are different from those expected from the crystal symmetry (e.g. the *z*-axis of A-site is the *c*-axis). However, the angles between H_{hf} and the incident γ ray are about 90°, which indicates that the magnetic moments align in the *c*-plane. The spectra in applied magnetic field can be interpreted by the canting of the magnetic moments. At H_{ex}=5 T, the observed fields (H_{obs}) are 30.3, 27.6, 27.4, and 17.9 T, respectively, suggesting that all the moments incline toward the applied magnetic field. With increasing applied magnetic field, the magnetic moments of B-site Fe incline upward, whereas those of A-site incline downward.
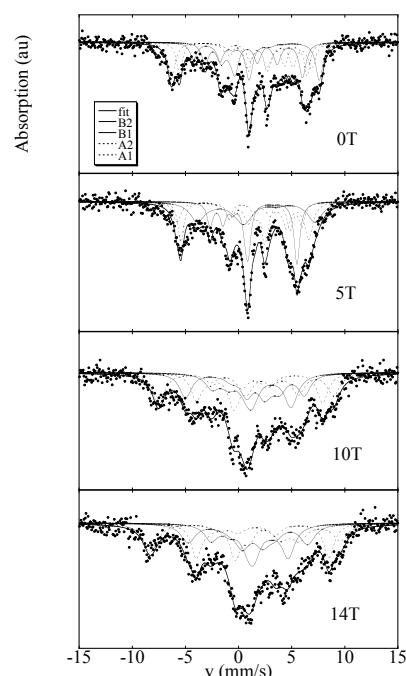

Fig.1. Môssbauer spectra of single domain Fe_2TiO_4 at 15 K in applied magnetic field.

REFERENCES:
[1] T. Yamanaka *et al.*, Phys. Rev. B,**80** (2009) 134120.
[2] Y. Ishikawa, *et al.*, J. Phys. Soc. Jpn. **31** (1971) 452.
[3] K. Kose, *et al.*, J. Phys. Soc. Jpn. **47** (1979) 77.
[4] S. Nakamura *et al.*, Hyperfine Int. **226** (2014) 267.